Electrochemical Nanogravimetric studies of Multi-walled Carbon Nanotubes and their Composites with Conducting Polymers

Chemistry M.Sc. Thesis

Colin E. Moore

Advisor: Professor Dr. György Inzelt

Eötvös Loránd Tudományegyetem, Budapest

Eötvös Loránd University, Budapest, Hungary

Faculty of Science

Institute of Chemistry

Department of Physical Chemistry

May 13, 2014

Acknowledgements

This work represents the culmination of my master's degree in chemistry at ELTE and was made possible only through the scientific guidance of Dr. György Inzelt. In addition, current and former members of the lab Balázs Berkes, Ákos Nemes, Balázs Broda and Szilvia Kasek added much needed support throughout. All of the professors who taught and or otherwise guided my studies cannot be thanked enough for their contributions to my skills as a chemist. My family was a constant source of encouragement helping me to achieve my goals. Finally, I would like to dedicate this work to my father Frank Howard Moore. It is in his memory that I strive to succeed.

Financial support of the National Scientific Research Fund (OTKA K100149) is acknowledged.

Table of Contents:

1. Introduction

The preparation, characterization and application of carbon nanotubes [1-5] and their composites including those with conducting polymers [6-26] have been in the foreground of research activity in electrochemistry in the last decades. This intense interest is understandable since several applications, especially in the fields of energy storage, batteries, fuel cells [19, 21] supercapacitors [4, 11, 13, 14, 16-18, 21, 22, 28] electroanalysis and biosensors [3, 12, 15] etc. have been accomplished. However, several fundamental properties of electrodes based on multi-walled carbon nanotubes (MWCNTs) and their composites with conducting polymers have not been studied in detail, yet. It was hoped that by using electrochemical quartz crystal nanobalance technique (EQCN) [27], the application of which has been somewhat neglected in the studies, except [5, 24, 25], may help to gain a deeper understanding of the electrochemical behavior of these systems, especially the potential dependent sorption phenomena.

In my thesis, the nanogravimetric results obtained for Au │ MWCNT electrodes and their "activation" during potential cycling will be discussed. In addition, results based on the adsorption / sorption of aniline and 6-aminoindole on MWCNT and the oxidative electropolymerization of adsorbed aniline and 6-aminoindole at Au │ MWCNT electrodes will be presented.

2. Literature background

2.1. Electrical double layer and adsorption phenomena

When discussing the chemistry of electrodes in aqueous environments, one must not neglect the effects of an electric double layer at the metal surface. In many electrochemical experiments, there is a disturbing effect due to the capacitive current which can obscure or even render unobservable electrochemical peaks in a cyclic voltammogram. As a result, we often seek to eliminate the effect of the double layer on our results. At other times, we try to enhance capacitive effect such as in the search for higher capacity and more efficient supercapacitors.

The first theoretical model of the electric double layer was produced in 1879 (Helmholtz) and assumed a compact layer of ions in contact with a charged metal surface. Due to deficiencies

in the ability of this model to accurately predict physical phenomena, Gouy and Chapman suggested a diffuse double layer where ions formed a double layer in a Boltzmann distribution extending some given distance from the electrode surface. More detailed descriptions of these effects can be found in the references [29-32].

Despite the extensive research that has been done on the subject, the structure of these double layers is not always simple to determine due to the effect of disturbing species, hydrated ions and different adsorption phenomena. One can have multiple species of analyte, solvent and electrolyte particles all taking part with different interactions to the electrode surface. In the case of platinum metal, carbon monoxide can covalently bond to two platinum atoms blocking active sites for the reduction of hydrogen. In this case, we have a disturbing species that will eventually block the activity of our electrochemical surface. Therefore, it is essential to study and understand these species and their effects on electrode surfaces.

2.2. Carbon nanotubes

Carbon nanotubes have been the subject of particular interest and intense study by research groups in different fields of scienc from engineering to biology. Carbon nanotubes are part of the fullerene family of carbon compounds and possess a large length to diameter ratio of up to 132,000,000:1 [33]. The tubes can be imagined one atom thick sheets of graphene rolled into long tubes. While it is possible to directionally generate these tubes in an ordered way[4, 8], they often stick to each other due to π-π interactions, forming bundles of nanotubes, especially in aqueous solutions. Carbon nanotubes can be synthesized using techniques including carbon arc discharge, pulsed-laser deposition or chemical vapor deposition. Using these techniques will form nanotubes with differing chemical and mechanical properties useful for a range of materials and for a variety of specific applications.

Due to the advantageous chemical, electrochemical and mechanical properties of MWCNTs, investigations for various applications have been carried out in detail as was discussed in the introduction section. However, it bears repeating that there is still uncovered territory in the field of the electrochemistry of carbon nanotubes. It is one of the goals of this investigation that some of these questions will be covered and explained.

2.3. Conducting polymers

The Nobel Prize in Chemistry 2000 was awarded to three researchers; Heeger, Macdiarmid and Shirakawa for their work on halogen oxidized poly(acetylene) in the 1970s. The novelty of their discovery was that it was in opposition to the classical interpretation of organic polymers as insulators. In fact, we use polymer insulators to great extent in our everyday lives as protective coatings for wires and other surfaces. Fortunately, spontaneous conductivity does not occur. However, it was discovered that through creating polymers with alternating single and double bonds within the macromolecular structure that one can produce intrinsically conductive polymers in the laboratory.

The preparation, characterization and application of electrochemically active polymeric films have been in the foreground of research activity in electrochemistry since the first report in 1978 [34]. This interest in research is understandable due to the possible uses of conducting polymers in the fields of energy storage, electrocatalysis, photoelectrochemistry, organic electrochemistry, bioelectrochemistry, electroanalysis, sensors, electrochromic displays, microsystem technologies, electronic devices, microwave screening and corrosion protection, etc. [26, 35].

2.3.1. Aniline and polyaniline

Aniline is a relatively simple chemical compound consisting of a phenyl ring coupled to an amino group. It is can be produced synthetically from benzene after the addition of a nitro group and its reduction. Aniline has been used since the 19th century when it was isolated from tar residues in the gas industry. In its most early uses, it was used as a dye in the textile industry [35]. However, as has often been the case with newly discovered toxic chemicals, it was not fully understood even as it was being mass produced and in 1862, the physician, Dr. Henry Letheby became interested in its pharmaco-kinetic properties after many of the factory workers fell ill. He actually reported the first formation of poly-aniline when he observed the formation of a bluish-green layer on the surface of an electrode upon oxidation. This color was eliminated upon the reduction of the layer [36]. The polymer description of the formed substance was not discovered, however, due to the fact that polymers and other macromolecules were not officially accepted by the scientific community until the 1920s. As was discussed in the introduction, in the last 150 years, polyaniline (PANI) has become the most widely studied and used conducting polymer [26, 35, 71, 72, 73].

2.3.2. Indole and polyindole

Indole is an aromatic heterocyclic organic compound with a bicyclic structure. The source of the term Indole comes from a *portmanteau* of *indigo* and *oleom*, or fuming sulfuric acid from which Indole can be isolated. The history of indole begins similarly to aniline with its first uses being in indole dyes. The first preparation of pure indole was performed in 1866 by Adolf von Baeyer when he reduced oxindole to indole using zinc powder [37]. Due to the structural similarity to alkaloids, research on indole intensified again in the 1930s and it remains an active research area to this day [38, 39]

Chemical and electrochemical oxidative polymerization has been executed [43, 44] to form polyindole. A wide range of applications for these polymers has been suggested including corrosion protection [41], batteries [44, 45], biosensors [46], and electrochromic devices [47-51]. The structure of polyindole has been a topic of intense discussion. Various papers have investigated the couplings of the indole monomers [52-55]. In addition, our lab has previously published a study [56] on poly(6-aminoindole) where the electro-deposition of 6-aminoindole was investigated by EQCN. In this report, we hope to compare the performance of poly(6-aminoindole) layers with composites prepared with MWCNTs.

3. Experimental Techniques

3.1. Cyclic voltammetry

Cyclic voltammetry or CV for short is the method of choice for many electrochemical measurements. These measurements were aided greatly by the invention of the three electrode potentiostat by Hickling in 1942 [57]. The technique can be used to determine the electrochemical properties of a variety of redox active compounds. The method consists most commonly of a three electrode system containing a working electrode, reference electrode and a grounded high surface area counter electrode. The principles of heterogeneous kinetics are the driving forces of the experiments with mass transport and electron transfer being possible limiting steps depending on multiple factors. It would be best to state that this section is not designed to be in any way comprehensive and for further references to the theories of linear sweep voltammetry it would be best to refer to the text book of Bard and Faulkner [30].

The principles of linear sweep voltammetry were elucidated independently and at almost the same time in 1948 by Randles and Sevcik [58, 59]. The Randles-Sevcik equation describes the effect of the sweep rate on the peak current (I_p).

$$I_p = 0.4463nFAc\left(\frac{nFcD}{RT}\right)^{1/2} \quad (1)$$

where n is the number of electrons transferred during the reduction / oxidation reaction, F is the Faraday constant in C mol^{-1}, A is the area of the electrode in cm^2, c is the concentration in mol dm^{-3}, v is the scan rate in V s^{-1}, D is the diffusion coefficient in cm^2 s^{-1}, R is the universal gas constant in J K^{-1} mol^{-1}, and T is the temperature in K.

The capacitive current is based on the charging of an electronic conductor. During scanning in a linear sweep experiment, the electrode surface becomes either positively or negatively charged uch like the plates of a normal capacitor. The charging current can be measured and is dependent on the rate of the linear sweep. This response most often manifests itself at the beginning of the CV response and can be described by Eq. (2).

$$I = v\,C_d \quad (2)$$

Where v is the scan rate in V s^{-1}, C_d is the capacitance in F and I is the capacitive current in A. This system can easily be approximated by using an R / C circuit where C_d is the capacitance of the electrode under investigation and R_s is the resistance of the cell in Ω. As the potential is applied at a constant sweep rate, we first see an increase in the current until it levels off to the current given from Eq. (2). These phenomena are described in detail on pp14-18 of [30].

The capacitance of a material can be determined from the area under a polarization curve (charge, q) divided by the scan rate according to Eq. (3). To find the specific capacitance (F g^{-1}) of a material, the capacitance of the layer is simply divided by the dry mass. This mass can be determined by subtracting the frequency of the clean electrode from the electrode containing the layer. This is only applicable in the case of the same electrode e.g. it is not possible to compare the dry mass of two different electrodes directly.

$$C = \frac{q}{v} \quad (3)$$

The Cottrell equation (4) describes the current response (I) in time (t) of an electrochemical reaction at an electrode surface.

$$I = \frac{nFAc_j^0\sqrt{D_j}}{\sqrt{\pi t}} \tag{4}$$

This response is also affected by the bulk concentration and diffusion coefficient of species j, c_j^0 in mol $m^{-3}$and D_j in m^2 s^{-1} respectively.

3.2. Electrochemical quartz crystal nanobalance (EQCN)

The Quartz crystal nanobalance (QCN) is a sensitive instrument used for measuring fine mass changes on a surface. As the name suggests, using EQCN, it is possible to measure mass changes of a material in the nanogram range. The technique is made possible by a piezoelectrically active crystal attached to a frequency counter. Piezoelectricity is a special property of certain materials where mechanical strain can be created through the application of a potential difference or, as in our case, mechanical changes to the crystal can result in an electrical signal. There is some application flexibility by using different crystal cuts and α-quartz is used in the majority of cases [27].

One can determine useful parameters from the oscillation frequency of the crystal. For instance, to calculate the mass change (Δm) of a film from a measured change in frequency (Δf) one can employ the Sauerbrey equation. Sauerbrey was a pioneer in the field of resonance frequencies of crystals. In Sauerbrey's original paper in 1959 [60], they were able to reach a sensitivity of 10^{-10} g on a dry substrate. The Sauerbrey equation can be written as

$$\Delta f = f_c - f_0 = -\frac{2f_0^2}{A\sqrt{\rho_q \mu_q}}\Delta m = -C_f \Delta m \tag{5}$$

where f_0 is the resonant frequency of the crystal in Hz, f_c is the frequency of the oscillator formed by the crystal and some film at its surface, Δm is the mass change in g, A is the piezoelectrically active crystal area in cm^2, ρ_q is the density of the quartz (2.648 g cm^{-3}), μ_q is the shear modulus of quartz and for an AT-cut crystal is equal to 2.947×10^{11} g cm^{-1} s^2, and C_f is the integral mass sensitivity in Hz g^{-1}.

In order to make quantitative measurements, the quartz crystals must first be calibrated to determine the frequency response to a deposition and dissolution of a well characterized chemical system. Most commonly, the determination of QCN sensitivity is carried out using

silver dissolution / deposition onto an electrode surface. This is useful due to the direct relationship between the charge measured in the CV and the frequency response and the absence of other disturbing interactions. A plot of the frequency vs. the charge consumed is generated from the deposition / dissolution reaction. From the slope of the plot, it is possible to determine the sensitivity of the crystal using Eq. (5).

It is easily achievable to combine EQCN with common electrochemical measurements such as galvanostatic, potentiostatic or cyclic voltammogramic measurements. By combining the techniques, it is possible to follow the charge consumed in the reaction and relate this to the moles of consumed reactant. This allows for the comparison of current responses and their corresponding frequency responses. This can be critical in mechanism elucidation from the molecular mass of the reacting species. By rearranging Eq. (5) it is possible to calculate the molecular mass of the reacting species by Eq. (6).

$$M = \frac{nFA\Delta f}{C_f Q} \tag{6}$$

where M is the molecular weight in g mol^{-1}, n is the number of electrons transferred during the reaction, F is the Faraday constant and A is the surface area in cm^2. In order for this equation to be valid, one must assume 100% charge efficiency as well as a uniform film generation over the whole surface of the electrode. Of course, in practice these two requirements are often not perfectly met. It is still possible to calculate the mass changes as long as one generates a film in a uniformly non-uniform way forming a random dispersion of material on the surface of the electrode.

3.3. Scanning electron microscopy

Scanning electron microscopy, or SEM for short, is a powerful tool for examining surface structures for a variety of nanostructured materials. The microscope scans the surface of a sample with a focused beam of electrons emitted from an electron source. Electron sources typically consist of a tungsten filament cathode due to its stability at extreme temperatures. The atoms on the surface of the sample will interact with the electron beam and electrons will be emitted back towards a detector. Most commonly, these secondary electrons are detected and from the angle and intensity of the reflected electrons it is possible to determine the depth of the surface and generate an image of its topographical features.

The early history of SEM measurements begins with Manfred von Ardenne in 1937. A special raster type scanning pattern was needed to obtain a magnified image and to reduce the chromatic aberration inherent to the microscope. This advancement made the imaging of surfaces by electrons possible. Further work was carried out by Zworykin and by groups at Cambridge in the 1950s and 1960s. A more detailed description of this history was presented by McMullan [61, 62].

Despite the power of SEM imaging, there are some inherent limitations to this technique. First of all, the sample must be electrically conductive and grounded. In our case, this poses no problem due to the conducting nature of the films under investigation, but for many samples that are either insulating or semi-conductive, further sample preparation is required. In the case of samples with limited conductivity, sample surfaces can be prepared by coating with an ultrathin layer of gold, platinum, chromium, or other appropriate conducting material by sputter coating or, alternatively, by high-vacuum evaporation. Without a conductive coating, non-conductive samples or samples with limited conductivity will often be altered or damaged by electron sputtering. In addition to the conductivity constraints, the sample chamber also must be under a high vacuum to prevent electrons from interacting with air. This vacuum creates a more efficient and suitable environment for the measurements and reduces noise in the system.

4. Materials and methods

4.1. Materials

Analytical grade H_2SO_4 and Na_2SO_4 from Merck and $NaNO_3$, NaCl, and KCl from Sigma-Aldrich were used as received. Multi-walled carbon nanotubes (Baytubes® C 150P, Bayer MaterialScience, Germany) were used. The main specifications of this product are as follows: C-purity: > 95 wt%, number of walls: 3-15, outer diameter: 13-16 nm, inner diameter: 4 nm, length: 1- > 10 μm, electrical conductivity: > 10^4 s cm^{-1}. Freshly distilled aniline (Merck) was used and all solutions were deaerated before the monomer was dissolved. 6-aminoindole (Sigma-Aldrich) was used as received and deaeration was performed similarly to aniline solutions. Doubly distilled water was used (Millipore water). During the electrochemical experiments, all solutions were purged with oxygen-free argon (purity: 5.0, Linde Gas

Hungary Co. Cltd.) and an inert gas blanket was maintained throughout the experiments. A saturated calomel reference electrode (SCE) was used.

4.2. Preparations, experimental conditions and instrumentation

4.2.1. Preparation of MWCNT layers

To prepare our MWCNT films, a 1:100 w/w mixture of MWCNTs in isopropanol was mixed using a Realsonic 57 ultra-sonicating water bath for two hours. A small volume of the mixture was drawn up into a capillary tube and deposited by gently tapping the end of the capillary onto the surface of the gold quartz crystal electrode. Using this technique, a uniform thin film was applied to the electrode surface. The isopropanol was allowed to dry overnight leaving a clean film of MWCNT.

4.2.2. Preparation of MWCNT-Aniline layers

We generated MWCNT-aniline films on the surface of gold electrodes in three ways. The first being the direct application of dissolved aniline in a solution of Ar purged 0.5 mol dm^{-3} H_2SO_4 at different concentrations. This was performed by placing the MWCNT covered gold crystal in a Teflon holder into the solution and waiting for a given time *ca.* 1 hr. This was followed by an oxidation in new Ar purged 0.5 mol dm^{-3} H_2SO_4 (thin films) or in the original aniline containing solution (thick films).

Additionally, we created a co-polymer by first sonicating the MWCNTs in pure aniline for two hours and then this was dropped onto the surface of the gold crystal electrode. This layer was allowed to sit in air overnight. The following day, the electrode was washed and the layer oxidized either buy CV or potentiostatic techniques. It should be noted that this procedure did not necessarily result in the generation of a co-polymer but that this term will be used simply as a descriptor of the film.

4.2.3. Electrochemical quartz crystal nanobalance measurements

A three-electrode cell was used. A gold wire was used as a counter electrode. The reference electrode was a sodium chloride saturated calomel electrode (SCE) separated with a double frit from the main compartment.

Five megahertz AT-cut crystals of one inch diameter coated with gold with titanium underlayer (Stanford Research Systems, SRS, U.S.A.) were used in the EQCN measurements. The electrochemically and the piezoelectrically active areas were equal to 1.37 cm^2 and 0.4 cm^2, respectively. The integral sensitivity of the crystals (C_f) was found to be 56.6×10^6 Hz g^{-1} cm^2, i.e., 1 Hz corresponds to 17.7 ng cm^{-2}.

The crystals were mounted in the holder made from Kynar and connected to a SRS QCM 200 unit. An Electroflex 450 potentiostat (Szeged, Hungary) and a Universal Frequency Counter PM6685 (Fluke) connected with an IBM personal computer were used for the control of the measurements and for the acquisition of the data.

Fig. 1. Photograph of EQCN holder, controller and crystals used in mass determination experiments from Stanford Research Systems model QCM200

Although the requirements (uniform and homogeneous surface layer) for the application of Sauerbrey equation are not perfectly met, on the basis of measured frequency values, a rough estimation can be made. This should not be an issue in the reported measurements and the relative values of Δf obtained for the incorporation of different ions and solvent molecules should be approximately correct.

4.2.4. SEM studies

The deposited layers were investigated by Focused Ion Beam Scanning Electron Microscope (FIB-SEM**)** type FEI Quanta 3D, The Netherlands.

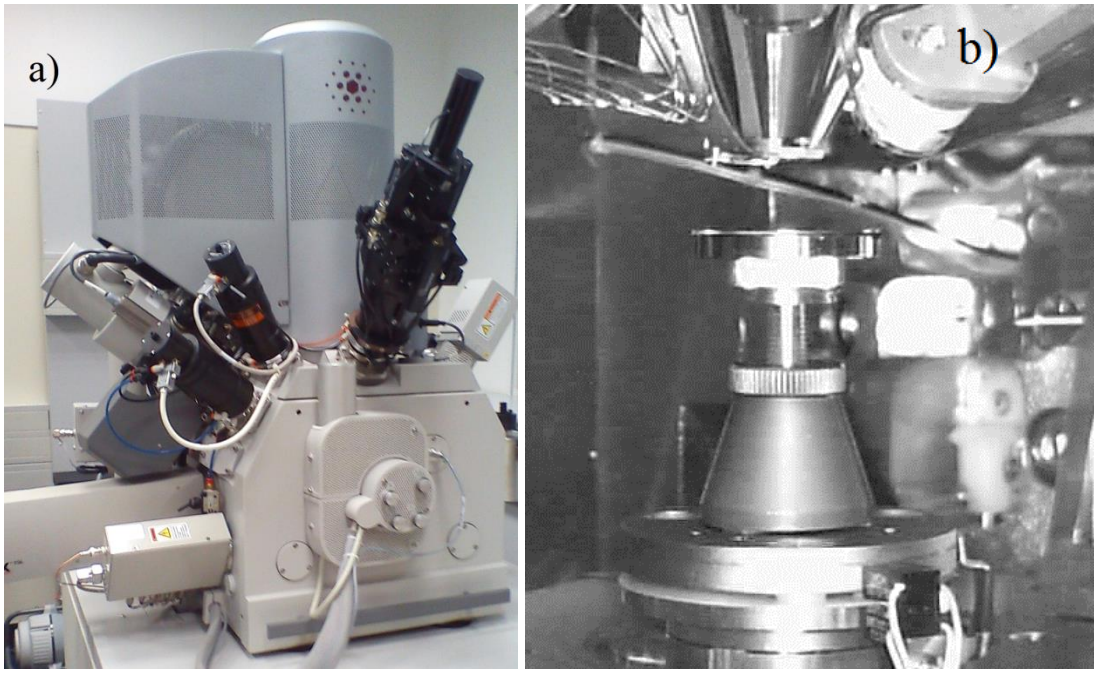

Fig. 2. Photograph of the Versa 3D FEI dual-beam FIB-SEM instrumental setup (a) and the measuring head (b) at the ELTE laboratory led by Dr. Havancsák Károly

5. Results and discussion

5.1. EQCN response of MWCNT films

5.1.1. EQCN and CV response of a gold electrode

We first measured a clean gold electrode using the EQCN to obtain a baseline for further experiments and to ensure the cleanliness of our system. At high potentials (*ca.* 1.6 V), the typical formation of a gold-oxide layer can be observed from the current waves as well as the frequency decrease (Fig. 3). At 0.8 V, the gold-oxide is reduced and an increase in frequency can be observed. Overall, the process results in a very small (less than 10 Hz) increase in the frequency of the crystal suggesting a removal of small amounts of contaminants present before the cycling on the surface of the gold electrode.

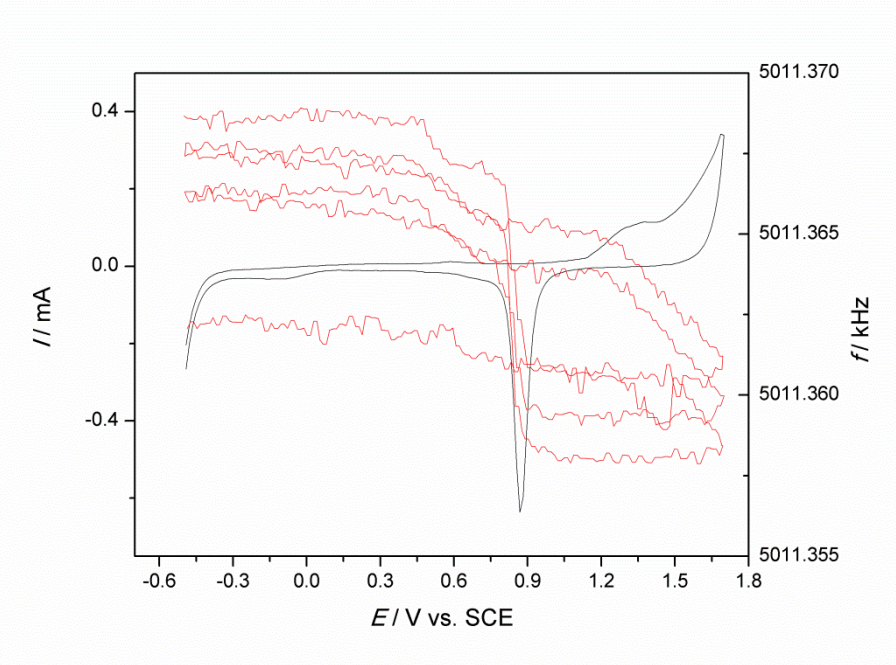

Fig. 3. Simultaneously obtained current and frequency response of an Au electrode crystal in the potential range from −0.5V to 1.7 V in Ar purged 0.5 mol dm^{-3} H_2SO_4 with a scan rate of 50 mV s^{-1}

5.1.2. Formation of a MWCNT film

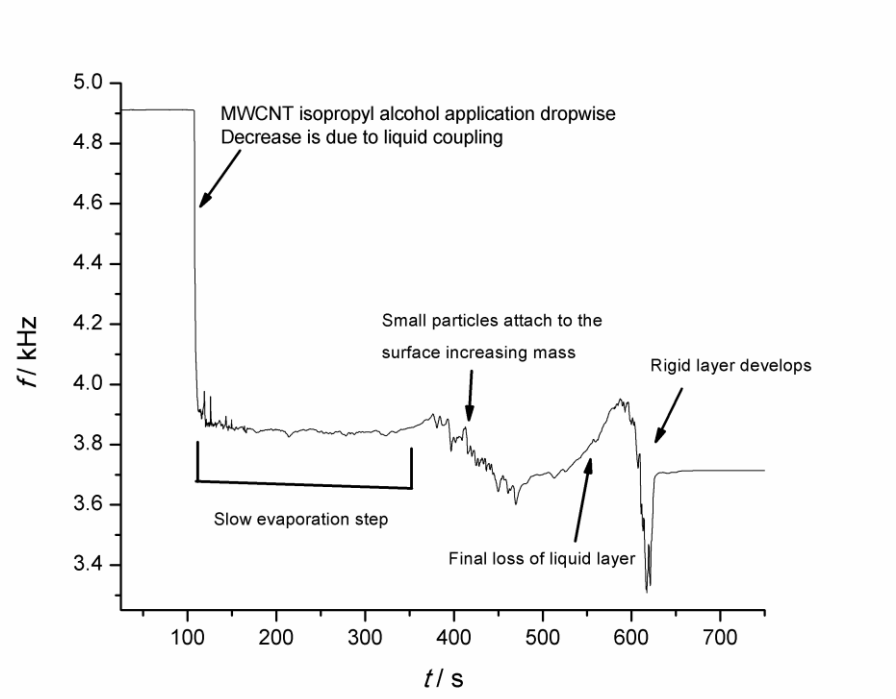

Fig. 4. Frequency changes during drying of an MWCNT-isopropanol sonicated suspension on a gold electrode quartz crystal. Application begins at *ca.* 100 s and ends at *ca.* 150 s

As seen in Fig. 4, placing a drop of the MWCNT isopropanol suspension on a gold surface results in an immediate decrease of the frequency due to viscous damping proportional to the density and viscosity of the liquid. The *ca.* 1,000 Hz is close to the expected value in this case [27]. During evaporation of the solvent, practically no change could be detected until the solution became concentrated when an oscillating behavior was observed. It can be assigned to competitive processes: evaporation of the liquid which causes a frequency increase and the deposition (attachment) of the MWCNTs to the surface which manifests itself in a frequency decrease. After the complete evaporation of isopropanol, a stable frequency value was measured. The total frequency change was *ca.* 1,200 Hz. By using Eq. (5), it corresponds to a mass change of 21.2 μg. The preconditions of the use of the Sauerbrey equation (uniform surface film) were not met in this case; however, the calculation should give a rather good approximation. It can be shown that if the surface layer covers the whole surface in a uniformly non-uniform manner, a reasonable value for the surface mass can be obtained. At least the values determined during further deposition and related to this mass change might be correct. Fig. 5 shows that MWCNTs covers the gold surface uniformly.

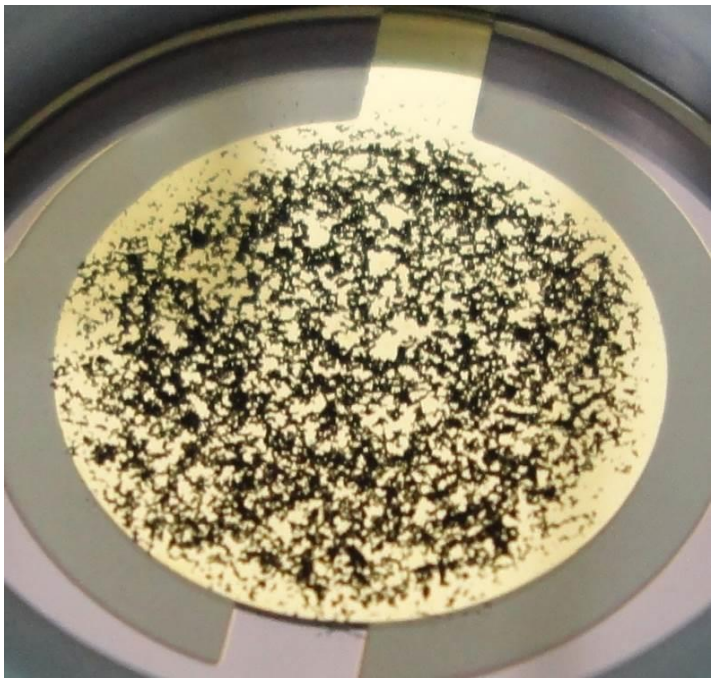

Fig. 5. Photo of a gold covered quartz crystal after the deposition of MWCNT and drying in air at ambient pressure

5.1.3. CV response of MWCNT films

In Fig. 6, we observed the mass and current response to voltammetric cycling of a gold surface covered with a MWCNT layer. The frequency response is the typically large (*ca.* 200 Hz) decrease seen in the first cycles after applying the MWCNT film. We see very little increase in capacitive current comparing a gold electrode to a MWCNT coated gold electrode. However, at positive potential limits higher than 0.8 V, the frequency change upon cycling is dramatic in the case of the nanotube layer. This is in contrast to the relatively stable and reversible frequency response of the gold electrode at the same potentials. This decrease is related to the swelling of the MWCNT film and independent of the reactions of the Au layer.

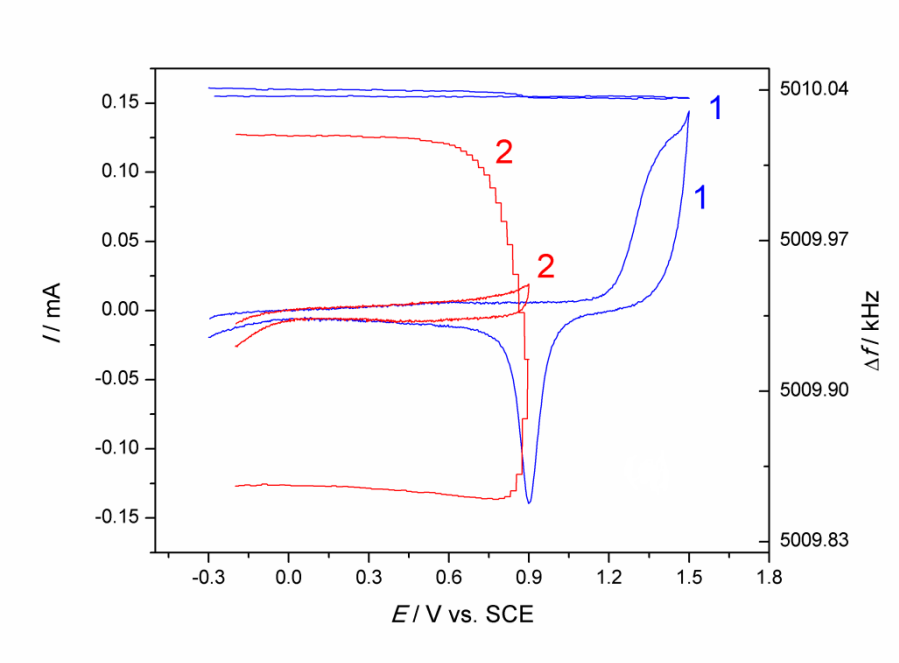

Fig. 6. (a) Simultaneously obtained current and frequency measurements of a clean gold electrode (blue, 1) (−0.3 V to 1.5 V) and Au-MWCNT film (red, 2) (−0.2 V to 0.9 V) 50 mV s^{-1}, 0.5 M H_2SO_4, Ar purged electrolyte. Measurements were made at 50 mV s^{-1} in 0.5 M H_2SO_4 after an Ar purge

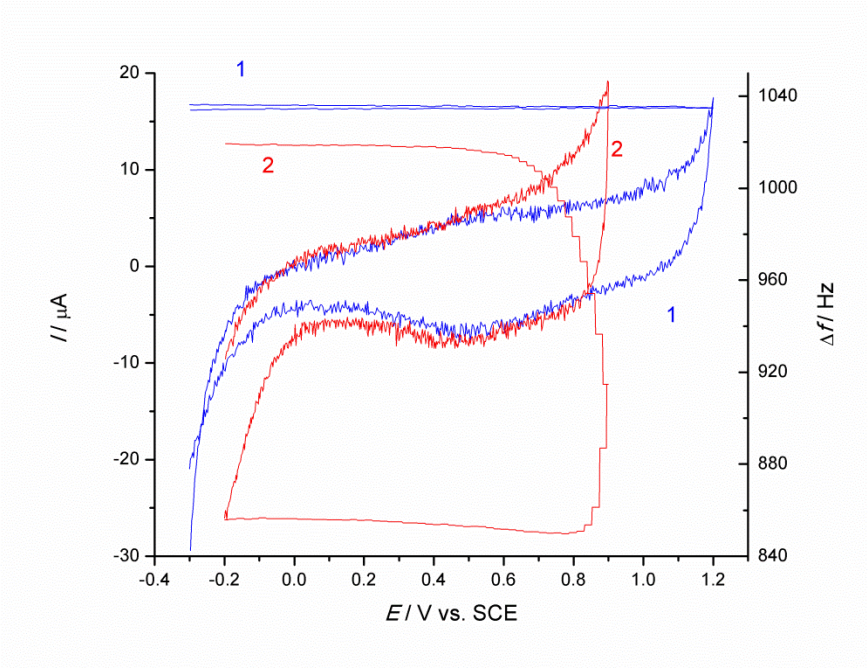

Fig. 7. Simultaneously obtained frequency and current response of pure gold (1, blue) from −0.3 V to 1.2 V and MWCNT (2, red) from −0.3 V to 0.9 V made at 50 mV s^{-1} in Ar purged 0.5 M H_2SO_4

It can be seen from Fig. 7 that capacitive current is not greatly increased by addition of MWCNT to gold alone. We will discuss this phenomenon further in section 5.1.4 but simply forming a layer of MWCNTs on the surface of a gold electrode is not adequate to obtain a strong capacitive response from the film.

5.1.4. MWCNT film conditioning

Carbon nanotubes are usually activated before their electrochemical investigation or application, e.g., in supercapacitors. The activation has been usually carried out by adding a strong oxidant to the suspension of CNT in acid media. Then agitation and elevated temperature have been applied for a long period of time [1, 4, 28]. The activation, which results in an increased specific capacitance, has been explained by the formation of hydroxy, oxo, and carboxy groups on the carbon nanotubes which make the nanotubes more hydrophilic. A similar effect has been reported by using an electrochemical treatment [4]. The phenomena occurring in the course of the electrochemical activation is one of the goals of this paper. It was indeed observed that when the positive potential limit was extended over 0.8 V; during cycling, the capacitive current slowly increased, and eventually a much higher capacitance could be achieved. What was really surprising was that an enormous mass

increase occurred above 0.8 V, even when the cyclic voltammograms did not change substantially; i.e., the increase of capacitance was still small (Fig. 6). In Fig. 7, the first cyclic voltammogram and the respective EQCN curve are displayed. It is evident that the effect observed is due to the MWCNT layer alone, and the sorption of anions on gold or even the gold oxide formation [70] play no role since the frequency change caused by these processes is orders of magnitude smaller.

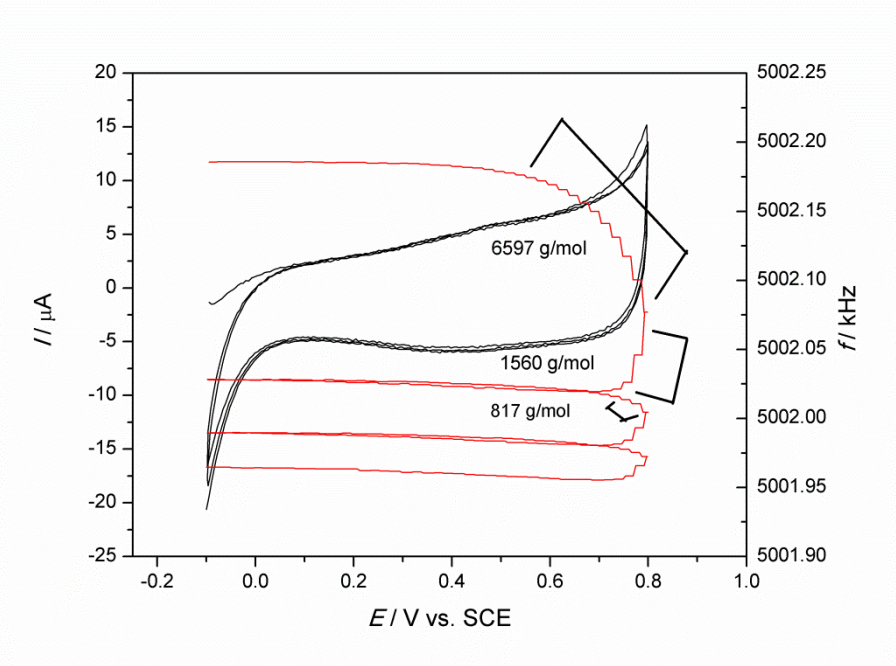

Fig. 8. Sequence of three subsequent cyclic voltammograms and the simultaneously detected EQCN responses during cycling of an Au │MWCNT electrode from −0.1 V to 0.8 V in Ar purged 0.5 mol dm^{-3} H_2SO_4 electrolyte at a scan rate of 50 mV s^{-1}

Performing multiple cycles of an Au-MWCNT film resulted in an activation of the MWCNT layer. The response observed in Fig. 8 is typical for a MWCNT film when compared to reports of chemical and electrochemical oxidative activation in other laboratories. We observed an increase in the capacitive current when compared to a gold electrode alone. This increase in capacitive current is a non-reversible change in the film. Even after the drying of the film, the same increase in the capacitive current is present when compared to the gold alone. The frequency response of the film, unlike the current response, becomes reversible after a high number of cycles and can be attributed to incorporation of water into the film. After drying the film in ambient pressure and temperature, the frequency of the film recovers back to within a few hundred hertz of the original dry frequency. This suggests that the bulk

of the frequency change is not due to a permanent oxidation of the film or incorporation of electrolyte but instead due to solvent swelling.

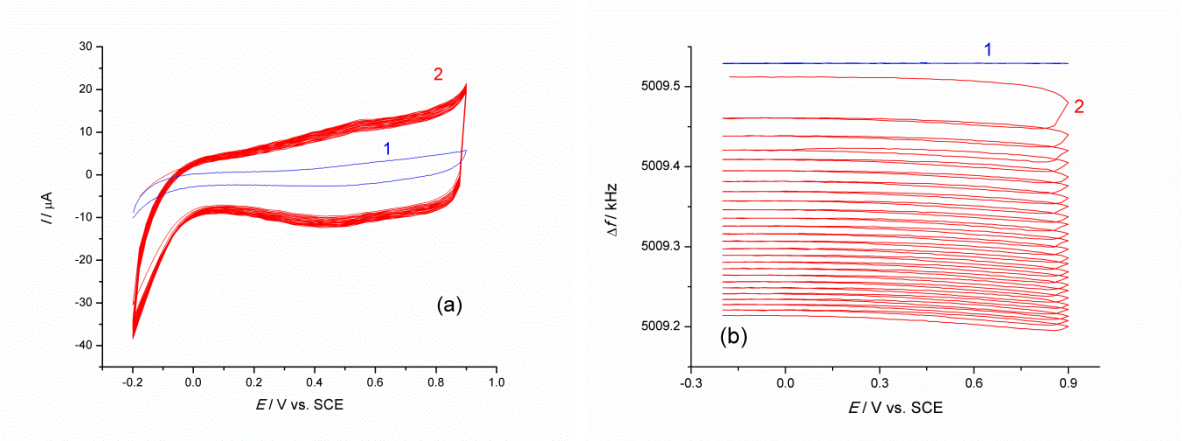

Fig. 9. Multi-cycle behavior of conditioned Au-MWCNT films and pure gold. The CV response (a) and frequency response (b) of a MWCNT film (red, 2) over 25 cycles from −0.2 V to 0.9 V and the response of a gold electrode (blue, 1) from −0.3 V to 1.2 V at 50 mV s^{-1} in Ar purged 0.5 mol dm^{-3} H_2SO_4 solution

5.1.5. Electrolyte effect on MWCNT cycling

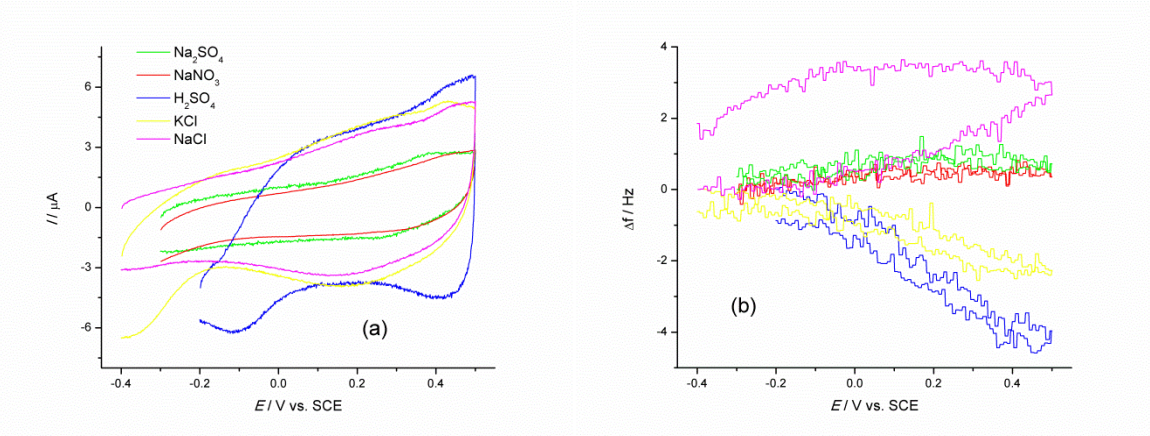

Fig. 10. Simultaneously obtained current (a) and frequency responses (b) of an Au electrode in Ar purged 0.5 mol dm^{-3} H_2SO_4, Na_2SO_4, $NaNO_3$, NaCl and KCl solutions at 20 mV s^{-1}. The positive potential limit was 0.5 V and the starting potential was between −0.4 and −0.2 V depending on the electrolyte

Removal of harmful electrolytes and heavy metals from waste water is a necessary process in industry before waste eluents can be reintroduced to the environment and increasingly, electrochemical methods are employed to achieve these goals [65-67]. To investigate the

uptake of electrolytes by MWCNTs, we recorded their frequency response over a narrow potential range (*ca.* −0.3 V to 0.5 V). Using the EQCN, it was possible to follow fine mass changes of the layer. The frequency response can be seen in Fig. 10. The effect was investigated under acidic as well as neutral conditions. We see a frequency maximum *ca.* 0.1 V in various electrolytes corresponding to a mass minimum of the film. This minimum is in fact the potential of zero charge (pzc) of the layer where the electrolyte concentration at the double layer is at a minimum. As a general trend, this mass increase / decrease became more pronounced with the addition of MWCNT films as compared to a clean gold surface. This could be due to the increased thickness of the effective double layer in the MWCNT film as compared to a gold electrode alone. However, because in the case of these ions, the real mass change caused by the specific adsorption is minor, other effects related to the nonspecific, electrostatic adsorption may dominate; mostly the change of the population of ions near the metal surface causing change in the viscosity and density of the solution layer [68]. Similar results have also been found for nanoporous carbon electrodes [69].

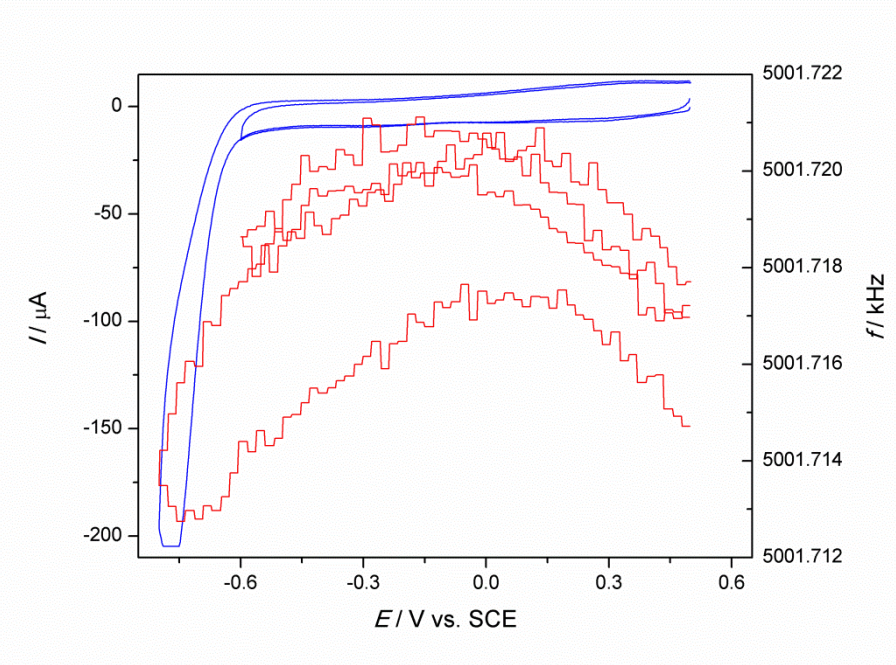

Fig. 11. Simultaneously obtained current and frequency response of an Au │MWCNT electrode in Ar purged 0.5 mol dm^{-3} $NaNO_3$ solution from 0.5 V to −0.6 V and −0.8 V at 50 mV s^{-1}

In Fig. 11, we see an example of the potential of zero charge determination on an Au-MWCNT film. As the potential is swept to more negative values, we see a frequency maximum between −0.06 V and 0.08 V by linear regression of the forward and reverse scans

respectively. These values are reproducible and were measured with several different electrolyte solutions. In addition, decreasing the negative potential limit resulted in the formation of hydrogen at the electrode surface and a non-reversible frequency response. This could be due to the reduction of oxo groups on MWCNTs that were generated during the activation process of the film. In Fig. 12, we compared the effect of different anions on the frequency response of the film. It can be seen that the sodium sulfate solution (red) has a slightly more positive pzc at the peak of the frequency curve. This is due to the differential mass of the hydrated ions and their effect on the viscosity of the solution close to the electrode surface.

To investigate the movement of solvated electrolyte molecules in the solution, we measured the scan rate dependence of the flow of anions and cations in and out of a MWCNT layer on a gold electrode. The results of these measurements are seen in Fig. 13. We observed the current and frequency response of the film at these different scan rates in the same electrolyte. The frequency changed with the same general pattern in all cases with a peak at around 0.1 V in Na_2SO_4 solutions. At faster scan rates, it is possible to see that the response has larger steps due to the movement of electrolyte in the double layer. We found that a scan rate of 20 mV s^{-1} was optimal for our experiments resulting in a smooth frequency curve. Scan rates higher than this resulted in inconsistent and difficult to interpret responses and noise became a disturbing factor due to instrumental constraints at lower scan rates. The capacitive current rose linearly with scan which was typical to other reports. This effect can be observed at around 0 V where the response of the film is purely capacitive without any disturbing peaks. Peak current also changed according to scan rate as can be seen in Fig. 13 *ca.* 0.4 V which is again typical for these scan rate experiments.

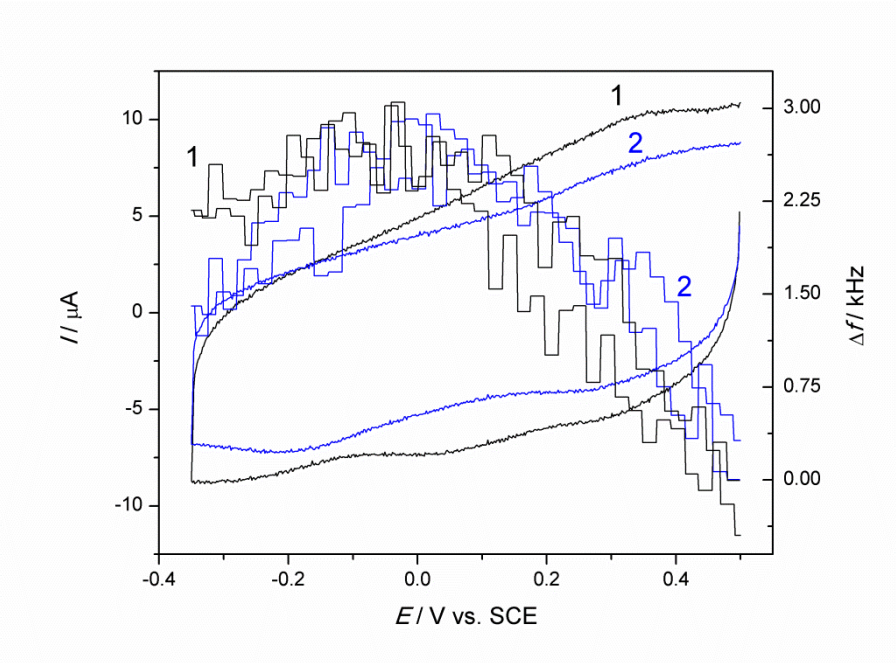

Fig. 12. Simultaneously obtained current and frequency response of an Au │MWCNT electrode in Ar purged 0.5 mol dm^{-3} $NaNO_3$ (black, 1) or Na_2SO_4 (blue, 2) solution from 0.5 V to −0.35 V at 50 mV s^{-1}

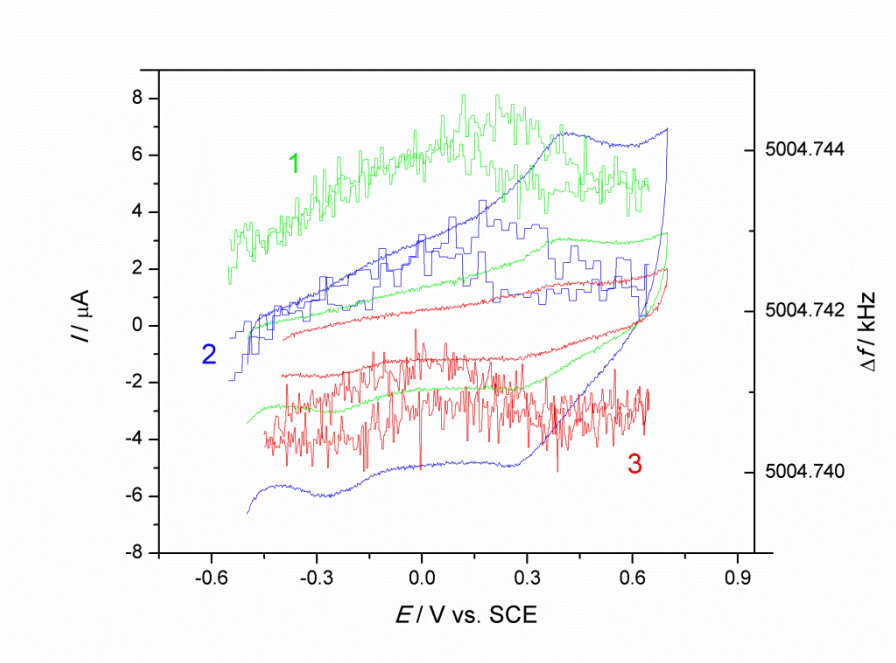

Fig. 13. Simultaneously obtained current and frequency response of an Au-MWCNT film cycled from −0.5 V to 0.7 V at scan rates of 10 mV s^{-1} (red, 3), 20 mV s^{-1} (green, 1) and 50 mV s^{-1} (blue, 2) in Ar purged 0.5 mol dm^{-3} Na_2SO_4

We determined the effect of supporting electrolyte concentration on the frequency response of our Au-MWCNT films in Na_2SO_4 and H_2SO_4 solutions. It can be observed from Fig. 14 that with increasing concentration of supporting electrolyte, a better defined peak frequency can be observed at *ca.* 0.1 V. At lower concentrations, a flat plateau can be seen from *ca.* -0.15 V to -0.30 V. This effect is due to the increase of the increasing concentration of sodium cations in the solution. This can be compared to the frequency response of the film when no sodium cations are present in the solution as seen in the case of sulfuric acid. Here the only difference is the cation species being sodium for Na_2SO_4 and the hydronium cation ion in the case of sulfuric acid. During the anodic portion of the scan, the electrode becomes negatively charged attracting positive ions. The mass effect of hydrated sodium ions is greater than the mass effect of hydronium ions on the double layer.

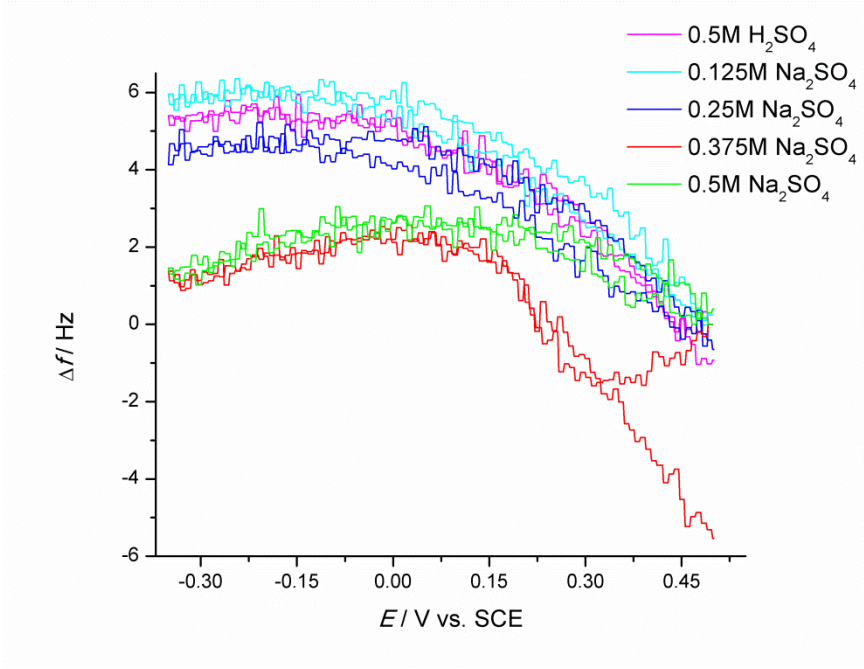

Fig. 14. Frequency response of an Au-MWCNT film when changing the supporting electrolyte concentration in a range of 0.125 to 0.5 mol dm^{-3} Ar purged Na_2SO_4. Sulfuric acid is shown as a comparison. A scan rate of 20 mV s^{-1} was used

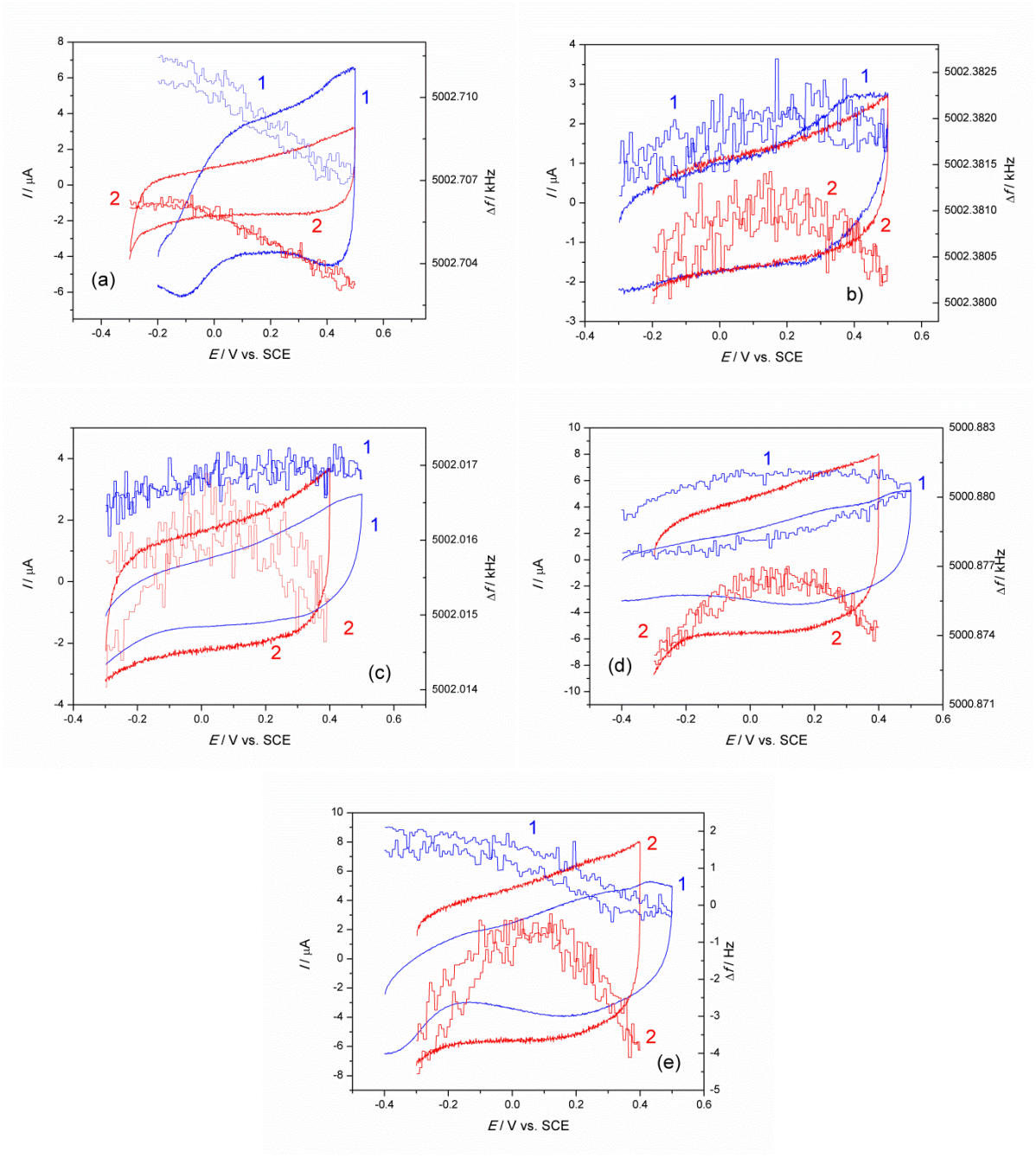

Fig. 15. The comparison of a gold electrode (blue, 1) and an Au | MWCNT electrode (red, 2) in various media. All measurements were taken at 20 mVs^{-1} all solutions were 0.5 mol dm^{-3} in Ar purged (a) H_2SO_4, (b) Na_2SO_4, (c) $NaNO_3$, (d) NaCl or (e) KCl electrolyte solution. Potential ranges were *ca.* −0.3 V to 0.5 V

We measured the current and frequency response of a gold electrode and our Au-MWCNT film in various electrolyte solutions at the same concentration of each solution. The results of these measurements can be seen in Fig. 15. In each case, there is a larger mass increase / decrease of the film in MWCNT as compared to gold alone. This effect is due to the

incorporation of either fully hydrated or partially hydrated ions into the layer. The ions can be incorporated into the electric double layer as well which would change the viscosity close to the electrode surface or directly into the film itself changing the mass of the attached MWCNTS. In addition, we see a slight increase in the capacitive current of the Au-MWCNT film as compared to the bare gold electrode. This increased capacitance was also observed in Figs. 6 and 7.

5.2. PANI covered MWCNT –Au electrodes

5.2.1. Adsorption of aniline on MWCNT

In previous studies, aniline nanotube composite layers have been prepared and characterized using various measurement techniques [8-12]. Thin composite films were investigated. However, it should be noted that these films were prepared by chemical polymerization with ammonium persulfate (APS) [8, 10]. Electrochemical preparations of the PANI films were carried out by using higher concentrated thick films of PANI-MWCNT polymerized directly from solution in [9]. In this investigation, we have performed for the first time a coupled cyclic voltammetric quartz crystal nanobalance study of both thick and thin electrochemically polymerized films. In Fig 16, we immersed a MWCNT layer into a solution of aniline resulting in the adsorption of small amounts of aniline to the film. This effect has a potential dependence and increasing the potential will increase the rate at which aniline adsorbs on the MWCNT film. The static potentials were chosen to be well below the polymerization potential of aniline on gold. In Fig. 17, we observed the concentration dependence of aniline adsorption at a fixed potential below the polymerization potential. The addition of higher aniline solution concentration during the adsorption also increased the rate of adsorption as would be expected. We added the aniline in three steps increasing the concentration from 5 mmol dm^{-3} to 10 mmol dm^{-3} and finally 15 mmol dm^{-3}. After the additions at 100 and 800 seconds, the slope of the frequency curve shows a marked increase indicating a faster rate of adsorption of aniline on the Au-MWCNT film.

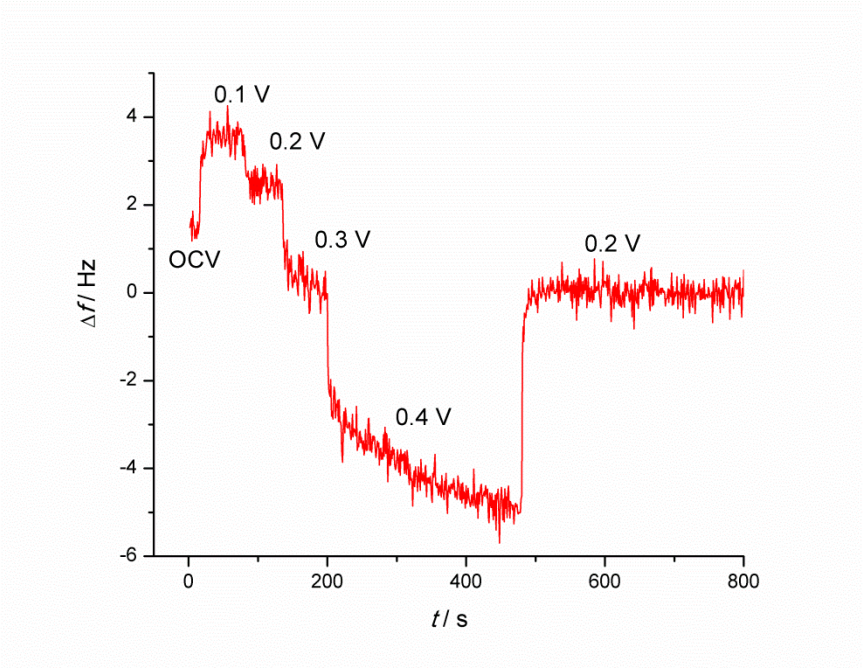

Fig. 16. The effect of the potential changes on the EQCN frequency response of an Au │ MWCT electrode in contact with a solution of 5×10^{-3} mol dm^{-3} aniline dissolved in Ar purged 0.5 mol dm^{-3} H_2SO_4 solution. The potential was stepped from the open circuit voltage to 0.1 V, 0.2 V, 0.3 V, 0.4 V and finally back to 0.2 V

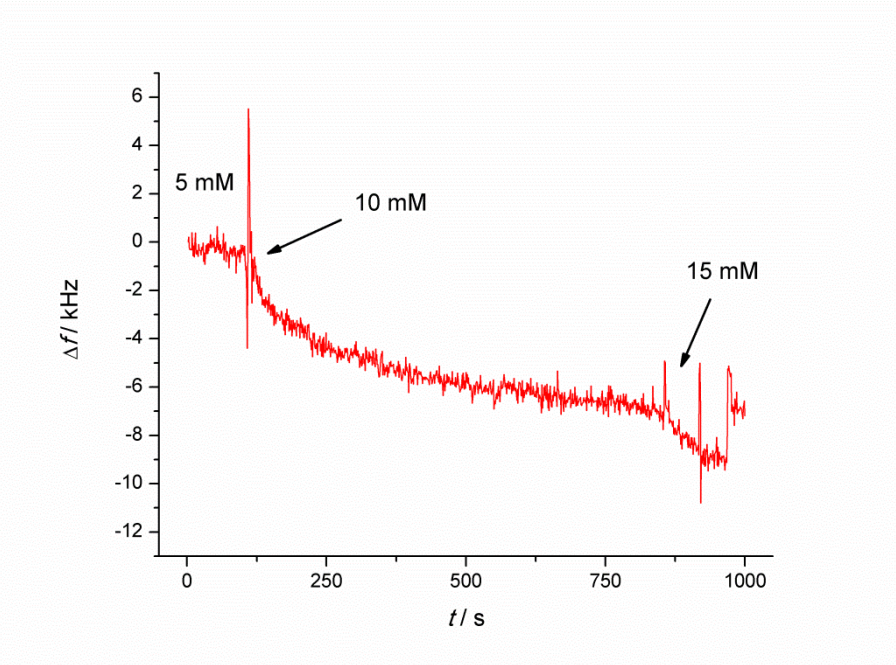

Fig. 17. Frequency response of an Au │MWCNT film in Ar purged aniline solution with 0.5 mol dm^{-3} H_2SO_4. From an initial concentration of 5 mmol dm^{-3}, the aniline concentration was increased to 10 mmol dm^{-3} at 100 s and 15 mmol dm^{-3} at 800 s

5.2.2. CV response of adsorbed aniline on MWCNTs

We prepared an aniline-MWCNT "co-polymer" film according to section 4.2.2 and this film was cycled while simultaneous frequency and current responses were measured. In Fig. 18, increasing positive potential limits were used. The frequency response is typical for a MWCNT film with a frequency decrease due to swelling being observed. In Fig. 19, the positive potential limit was set to the polymerization potential of aniline. There was a large increase in the capacitive current of the "co-polymer" vs. MWCNT or gold alone. This effect seems to be dependent on the amount of aniline present in the film. It should be noted that there are two waves, one on the forward sweep and one at the reverse sweep that appear in the cyclic voltammogram of our PANI-MWCNT-Au electrode. These appear at 0.5 V and 0.45 V respectively and are typical for the initial cycles of a polyaniline film. They are most likely due to the oligomerization of the aniline as a step prior to the full polymerization of the film.

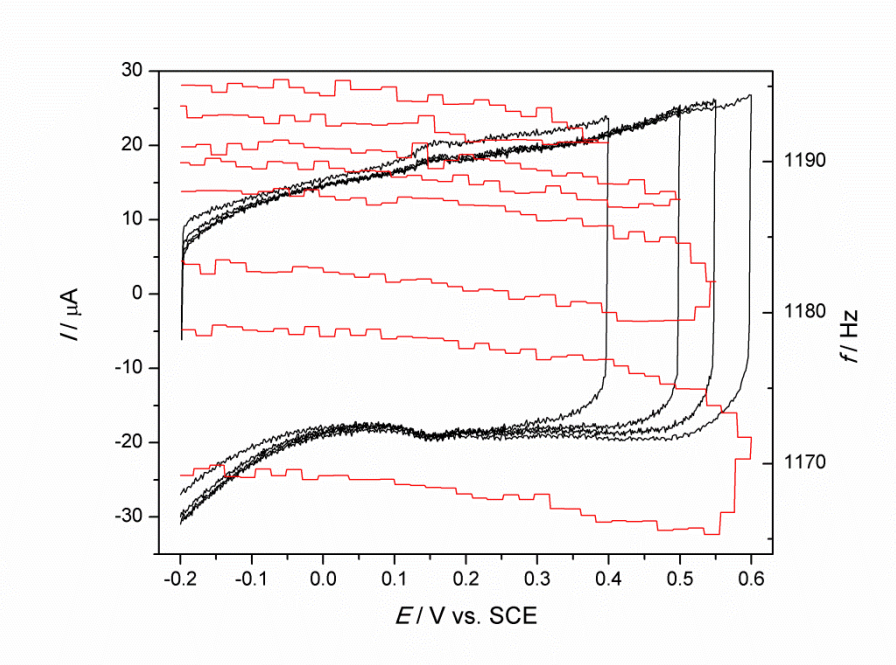

Fig. 18. Simultaneously obtained frequency and current response of aniline adsorbed on Au-MWCNT film at 50 mV s^{-1}.From an initial potential of −0.2 V the film was cycled to a positive potential limit of 0.4 V to 0.6 V over the course of four cycles

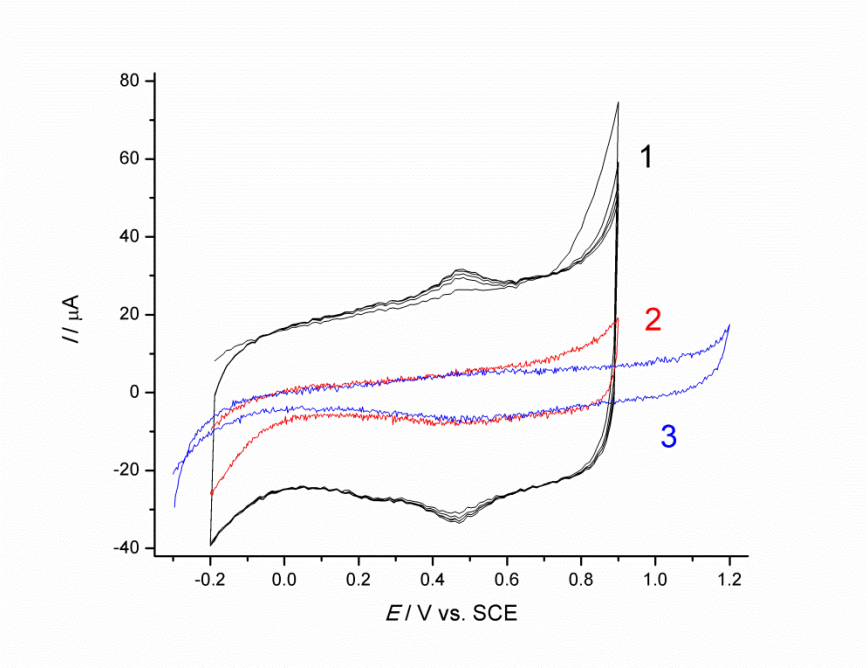

Fig. 19. Current response to cycling of aniline "co-polymer" (black, 1) from −0.2 V to 0.9 V, MWCNT (red, 2) from −0.2 V to 0.9 V and pure gold (blue, 3) from −0.3 V to 1.2 V. Carried out in Ar purged 0.5 mol dm^{-3} H_2SO_4 with a scan rate of 50 mV s^{-1}

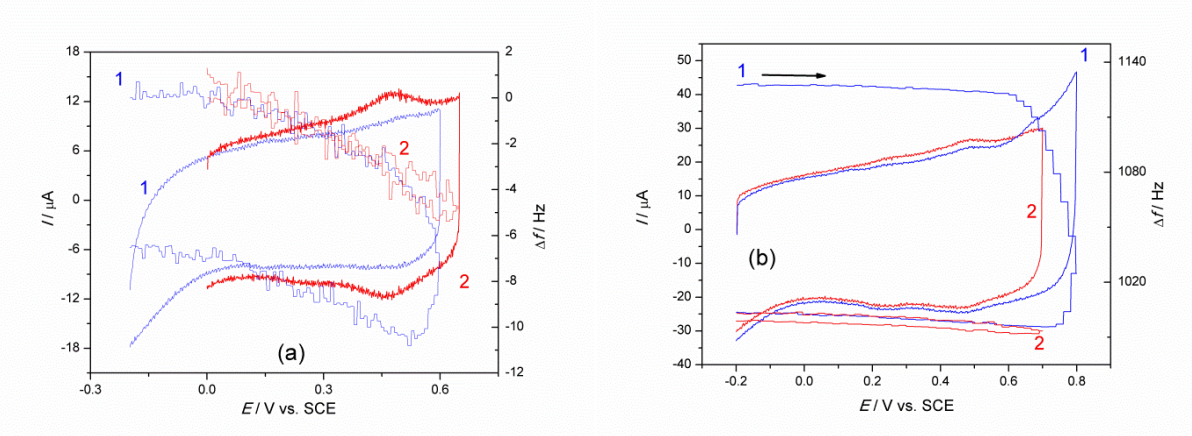

Fig. 20. Simultaneously obtained current and frequency response of sonicated aniline MWCNT films (a) Pre (blue, 1) and post (red, 2) (after reaching *ca.* 0.8 V) PANI-polymerization cycles. (b) Pre- (blue, 1) and post-(red, 2) polymerization of aniline/MWCNT film. All cycles were performed in Ar purged 0.5 mol dm^{-3} H_2SO_4 solution at 50 mV s^{-1}

In Fig. 20, we observed the difference between the pre-polymerized film (i.e. cycles of the film before reaching the polymerization potential of *ca.* 0.8 V) and one cycle from after polymerizing aniline on Au-MWCNT. The post polymerization CV (Fig. 20 b, curve 2) shows the same oligomeric waves seen in the previous Fig. 19 and these waves are certainly

not as prominent in the pre-polymerized film. In addition to the formation of waves, we see a slight increase in the capacitive current between the two cycles. The most striking feature is the change in the frequency response of the film. Pre-polymerization, we see the typical swelling response of the carbon nanotubes resulting in a large frequency decrease. This was seen previously in the multi-cycle Fig. 8 where a large decrease in the frequency occurs in the range of 0.6 V to 0.8 V on clean Au-MWCNT films. After polymerization, we can see that this effect is blocked by the resistance to swelling within the film. There are two possible explanations for this behavior. The MWCNT network on the surface of the gold is only loosely bound with no cross linking between the nanotubes themselves. The aniline could cause a cross-linking between the individual MWCNTs preventing swelling. They also contain pores that can accept cations, anions or water molecules affecting the mass of the layer. The polymerization of aniline could also cause a clogging of these pores restricting the swelling. Additionally, it is possible that a combination of the two is the cause of this response.

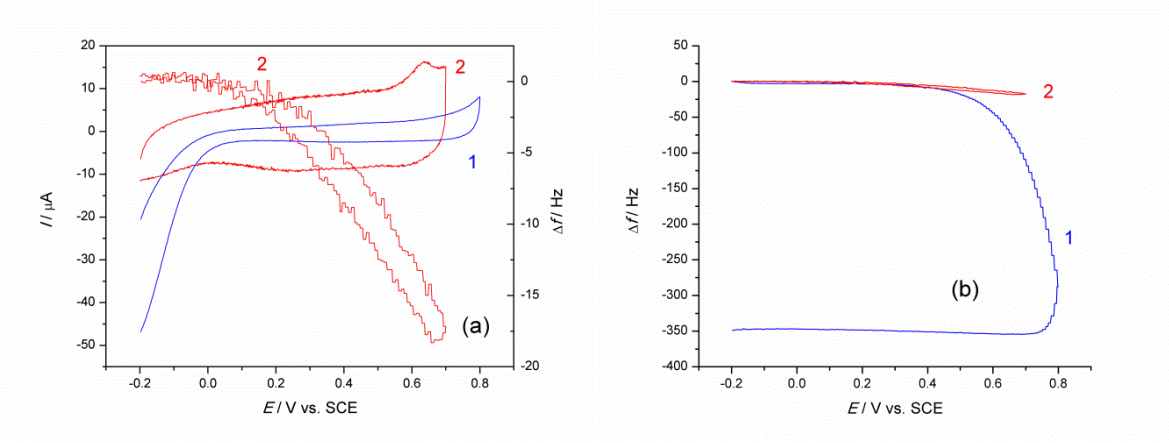

Fig. 21. The (a) cyclic voltammograms and the simultaneously obtained EQCN frequency responses obtained for an Au │MWCT electrode from −0.2 V to 0.8 V (blue, 1) and an Au │MWCT electrode after the adsorption of aniline (red, 2) (b) shows both frequency responses (see Fig. 17) from −0.2 V to 0.7 V in Ar purged 0.5 mol dm^{-3} H_2SO_4 solution at a scan rate of 20 mV s^{-1}

In Fig. 21, the current and mass response of an Au-MWCNT film was compared to an Au-MWCNT-PANI film upon cycling. The typical mass response of the MWCNT film was observed by the frequency decrease of the film beginning at about 0.7 V. This response is suppressed by the aniline composite and a reversible frequency response can be observed. This change in response can be attributed to reduced swelling of the film as previously

discussed. In Fig. 22, we saw a difference in the cyclic voltammogram before polymerization and afterwards. The green CV was taken before the positive potential limit was set to polymerization potentials and it shows the response of the adsorbed aniline mostly in a featureless CV consisting of a purely capacitive response. The blue CV shows much the same response on the forward scan, but on the reverse scan, we see the formation of two waves; one at *ca.* 0.5 V and the other at *ca.* 0.2 V. Finally, the red scan shows new features of the oligomerized-aniline on the surface of the Au-MWCNT film and the reverse scan mirrors the polymerization step confirming that a chemical change has taken place on the film.

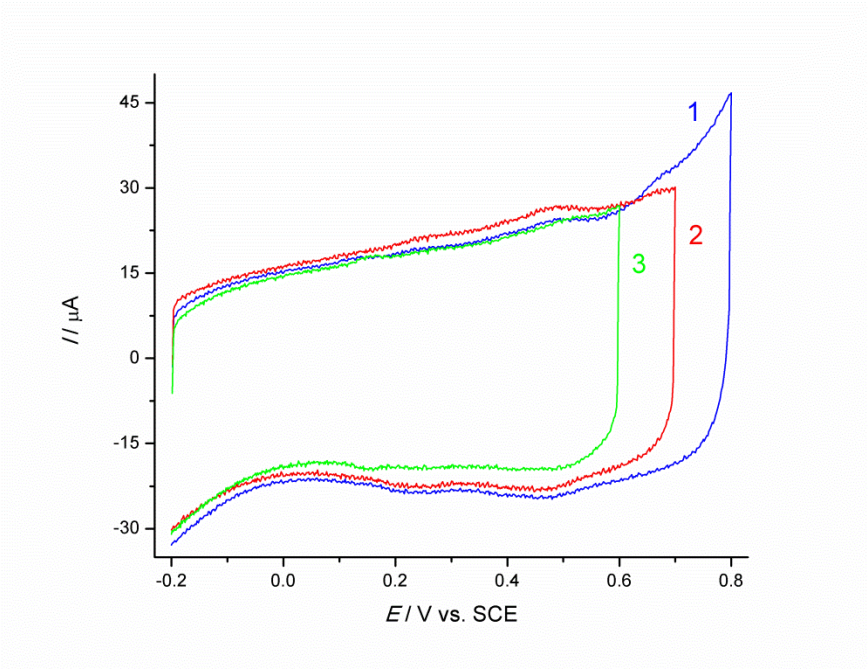

Fig. 22. Current response of an aniline adsorbed Au-MWCNT film before polymerization (green, 3) from −0.2 V to 0.6 V, during the polymerization step itself (blue, 1) from −0.2 V to 0.8 V and the cycle taken after polymerization (red, 2) from −0.2 V to 0.7 V. Cycles performed in Ar purged 0.5 mol dm^{-3} H_2SO_4 at 50 mV s^{-1}

In Fig. 23, we have compared the cycle of a PANI-MWCNT-Au film against the MWCNTs alone. In the case of the MWCNT film, we observe the typically large frequency decrease of the film upon electrochemical activation that was discussed in section 5.1.4. However, in the case of the MWCNT-adsorbed aniline film, we do not observe such a dramatic mass increase even at the higher potentials reached in Fig. 23. After the oxidation of aniline, the extensive swelling of the MWCNT layer cannot be observed.

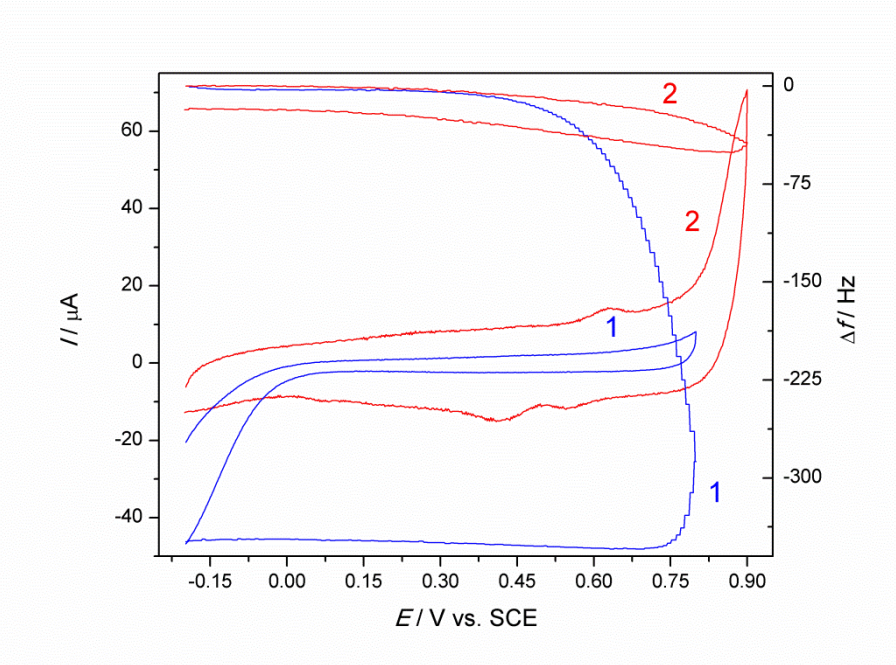

Fig. 23. Simultaneously obtained EQCN frequency during cycling of an (red, 2) Au │MWCT-polyaniline electrode in an Ar purged 0.5 mol dm^{-3} H_2SO_4 solution between −0.2 and 0.9 V. The curves obtained for the (blue, 1) Au │MWCT from −0.2 V to 0.8 V are also displayed with a scan rate of 20 mV s^{-1}

In Fig. 24, we have an example of a thin film of aniline on the surface of MWCNTs. In this case, we have placed the oxidized thin film in a solution of fresh sulfuric acid. We observe a reversible frequency response to cycling as is expected. A minor pair of waves appear at the usual potential of the leucoemeraldine ⇆ emeraldine transition of PANI, i.e., between 0 V and 0.1 V. A dominant pair of waves can also be seen in the potential range of 0.47 V and 0.5 V. The response of the polyaniline film varied widely with the ammount of aniline monomer applied to the MWCNT film. This is seemingly due to the differential response of polyaniline and aniline oligomers to potential cycling.

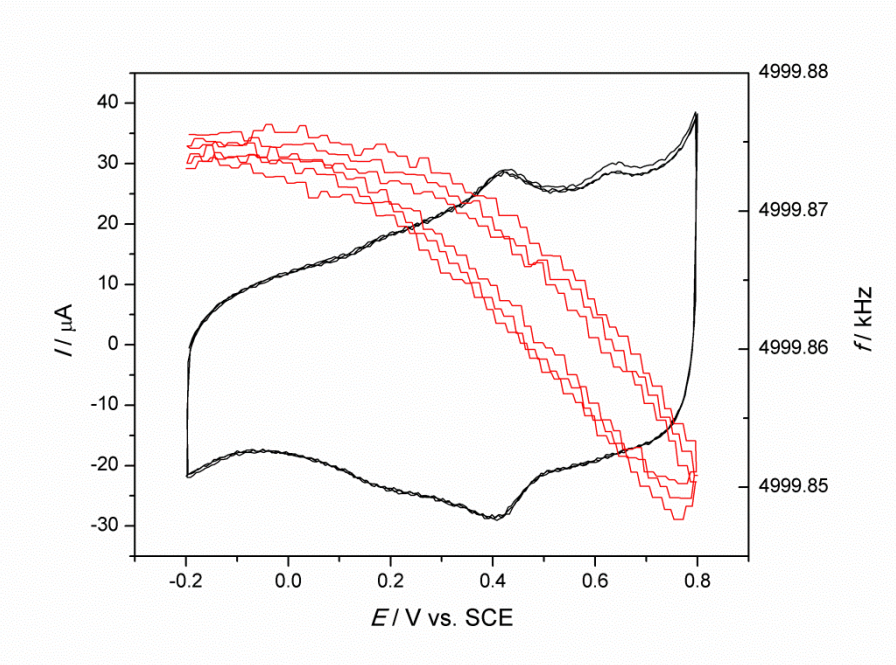

Fig. 24. The cyclic voltammograms and the simultaneously obtained EQCN frequency responses during cycling from −0.2 to 0.8 V of an Au │MWCT-polyaniline electrode in 0.5 mol dm^{-3} H_2SO_4 solution with a scan rate of 50 mV s^{-1}

5.2.3. PANI-MWCNT composites

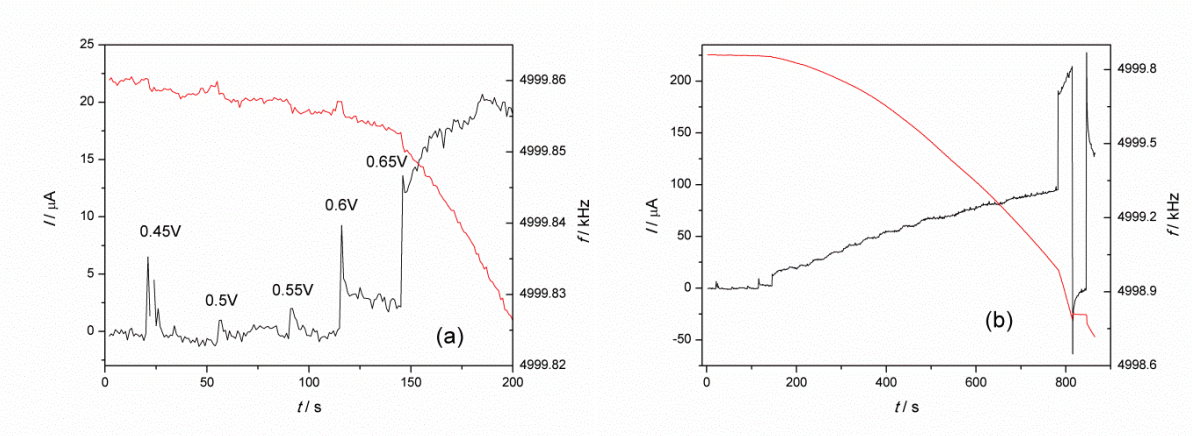

Fig. 25. Simultaneous current and frequency response of an Au-MWCNT film in aniline solution of 15 mmol dm^{-3} and Ar purged 0.5 mol dm^{-3} H_2SO_4 at chronoamperometric measuring conditions. The initial potential was stepped from 0.45 V, 0.50 V, 0.55 V, 0.60 V and finally to 0.65 V where the polymerization was continued for 700 seconds. There is a close-up (a) of the overall film generation (b)

In Fig. 25, we measured the deposition of aniline on an Au-MWCNT electrode using a chronoamperometric technique coupled with EQCN in a sulfuric acid solution. These conditions were typical of previous reports of aniline polymerization [36, 70-73]. We polymerized at 0.65 V for 700 seconds depositing a total of 1,400 Hz or approximately 24 μg to the surface of the Au-MWCNT electrode. There was no observed aniline formation on the surface of the gold even after a thick film deposition (*ca.* 1,000 Hz) by polymerization. This could be due a low overpotential for aniline oligomer formation on MWCNTs as compared to the relatively high overpotential needed for the oligomerization of aniline on a gold surface. This was readily observed by eye in the lab and can be seen in the photograph of one of the formed layers (Fig. 26) as well as a closer look by SEM (Fig. 29 a).

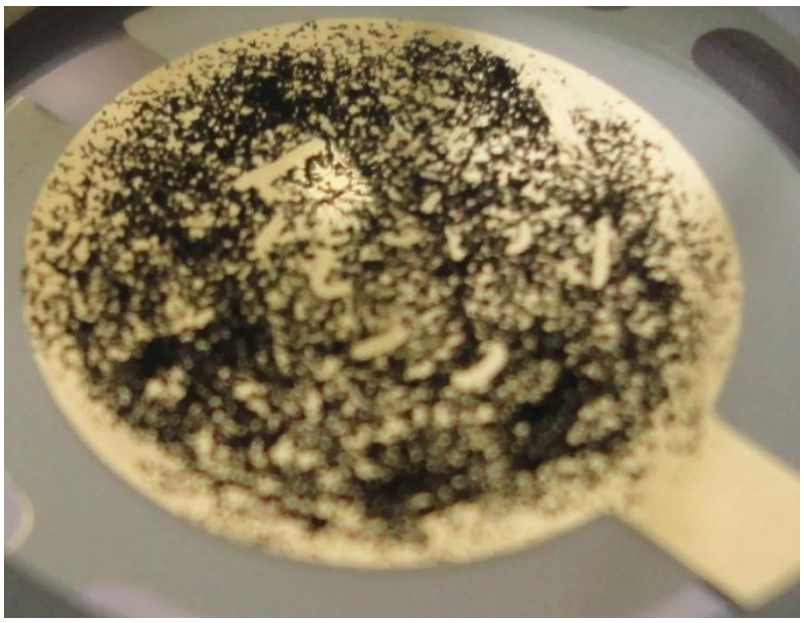

Fig. 26. Photograph of a PANI-MWCNT film on a gold covered quartz crystal

Fig. 27 shows the response of our film on the first cycle after chronoamperometric generation of aniline on Au-MWCNT film. It is a typical electrochemical response to cycling for a PANI film as previously observed by various groups. In this case, we have left the electrode in the solution containing dissolved aniline. Therefore, once polymerization begins at *ca.* 0.55 V, the frequency change is a permanent mass change to the film unlike the reversible response between 0.2 V and 0.55 V which is a reversible change in the film mass. The wave at 0.15 V is the electrochemically reversible oxidation of the film and on the reverse scan, the wave at −0.05 V is the electrochemically reversible reduction of the PANI film. As was previously mentioned, these waves are typical and comparable to what has been observed by other groups.

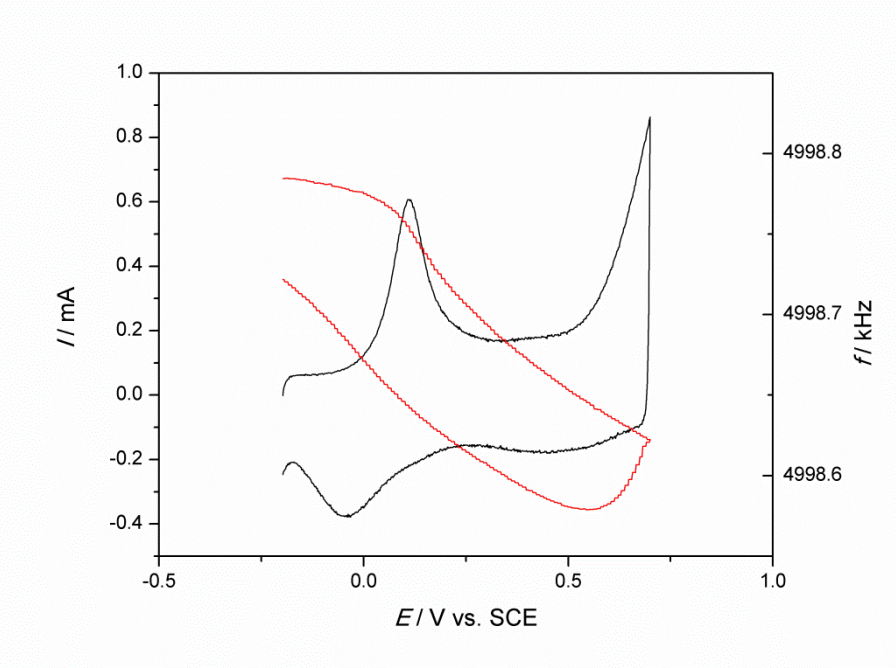

Fig. 27. Simultaneously obtained current and frequency responses of a PANI-MWCNT-Au film cycled from −0.20 V to 0.65 V in 15 mmol dm^{-3} aniline dissolved in 0.5 mol dm^{-3} H_2SO_4 at 20 mV s^{-1}

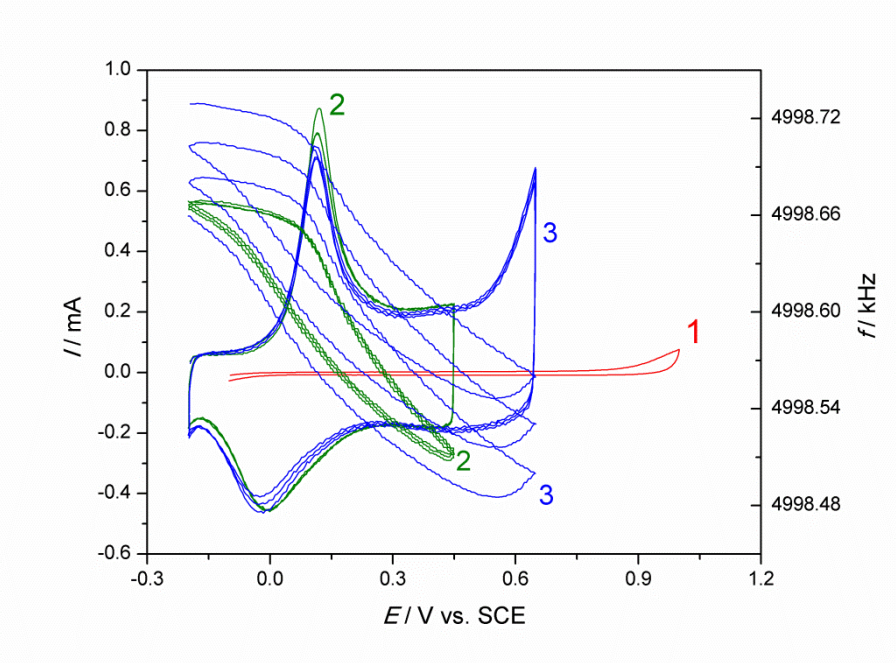

Fig. 28. The cyclic voltammograms and the simultaneously obtained EQCN frequency responses of an Au | MWCNT-polyaniline electrode in 5 mmol dm^{-3} aniline dissolved in 0.5 mol dm^{-3} H_2SO_4 solution (curves 2 and 3 from -0.2V to 0.45 V and −0.2 V to 0.7 V, respectively) and Au | MWCNT (1) in 0.5 mol dm^{-3} H_2SO_4 with a scan rate of 20 mV s^{-1}

In Fig. 28, we were able to reproduce the characteristic CV response of a PANI film. Curves marked 1 are of a clean MWCNT layer used as a comparison. In the curves marked number 3, we reach the polmerization potential of aniline. In three successive cycles, we observe a thickening of the PANI film on the surface of MWCNTs. The current response reflects this oxidation with a peak current reaching *ca.* 0.8 mA. The curves marked 2 are cycled in a shorter range and the frequency response for the film is completely reversible. In this case have the typical pair of peaks at *ca.* -0.05 V and 0.15 V for the reverse sweep and forward sweep, respectively.

5.2.4. SEM investigations

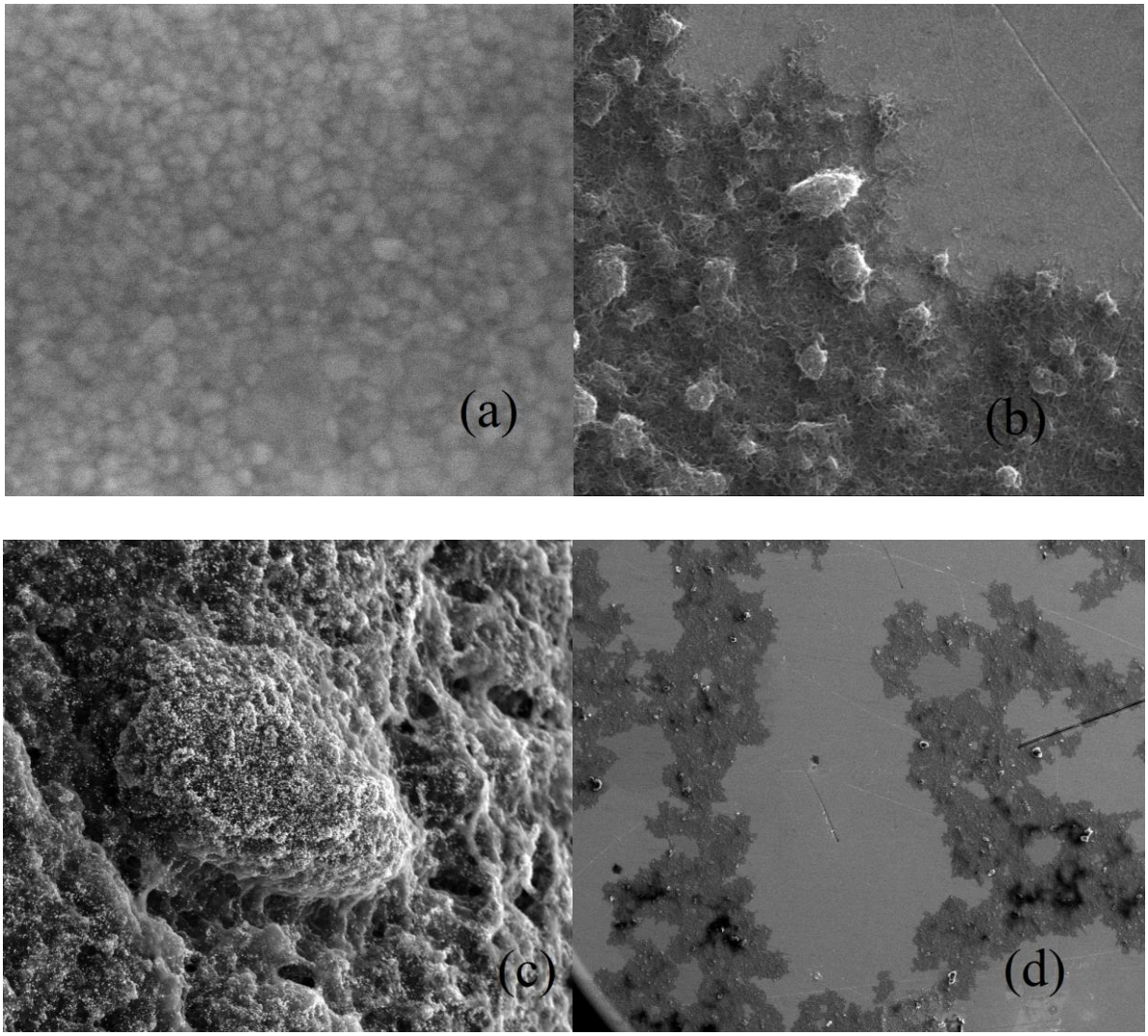

Fig. 29. SEM images of a (a) clean gold surface at 100,000 × magnification, (b) MWCNTs on a gold surface at 10,000 × magnification, a (c) PANI film at 2,500 × magnification and a (d) PANI-MWCNT film at 100 × magnification

In Fig. 29 a, an amorphous gold surface can clearly be seen. This electrode had been first covered with MWCNTs and cycled. This was followed by aqueous PANI film generation of *ca.* 1,400 Hz by potentiostatic methods. The clean surface of the gold indicates that aniline oligomer formation occurs at lower overpotentials on the MWCNTs than on the surface of the gold. This caused the polymerization of aniline to take place exclusively on the surface of the nanotubes attached to the electrode surface. The gold surface remained clean as was observed both by eye in the laboratory Fig. 6 and upon closer inspection by scanning electron microscope Figs. 29 a, b and d at different magnifications. Fig. 29 c is an SEM image showing the morphology of a normal PANI film.

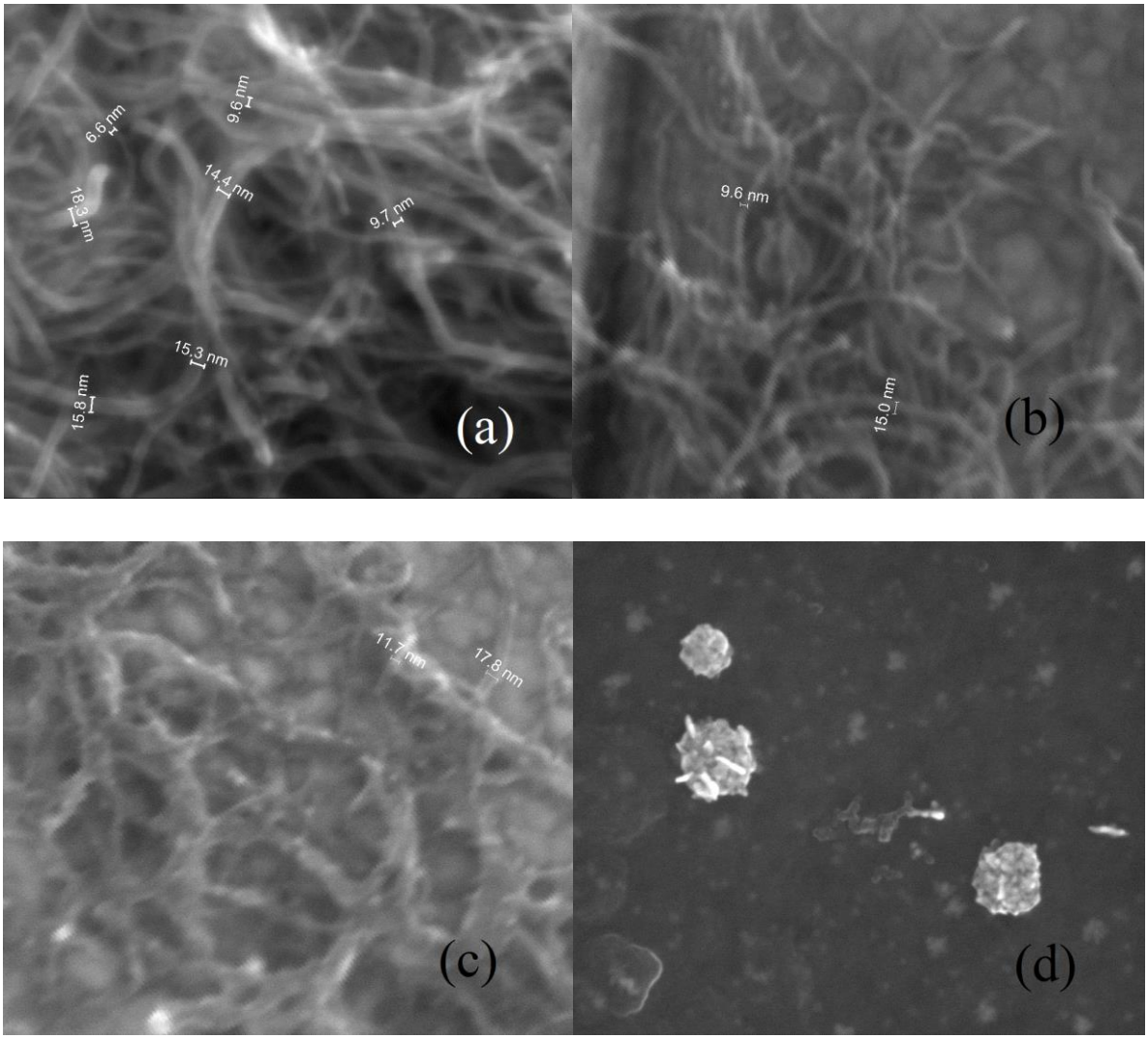

Fig. 30. SEM images of (a) MWCNTs at 250,007 × magnification, (b) MWCNTs with adsorbed aniline at 200,000 × magnification, (c) a MWCNT-PANI film at 200,000 × magnification and a (d) poly(6-aminoindole) film at 100,000 × magnification

The images in Fig. 30 show the variation between Au-MWCNT and Au-PANI-MWCNT films under a scanning electron microscope. The thicknesses of selected nanotubes were measured using the analysis software of the SEM. The thicknesses of MWCNTs alone were variable due to the nature of the acquired nanotubes having multiple walls. Nonetheless, it can be seen that the thickness of the nanotubes in Fig. 30 a (from 6.6 nm to 15.8 nm) increased slightly after the adsorption of aniline in Fig. 30 b (from 9.6 nm to 15.0 nm). After the formation of PANI on the surface of the MWCNTs, we observe a dramatic thickening of the nanotubes in Fig. 30 c (measured 11.7 nm and 17.8 nm). Additionally, we have presented in Fig. 30 d, an SEM image of a poly(6-aminoindole) covered gold electrode. We will discuss the characterization and behavior of poly(6-aminoindole) films in section 5.3.

5.3. Poly(6-aminoindole) MWCNT covered electrodes

5.3.1. Adsorption of 6-aminoindole

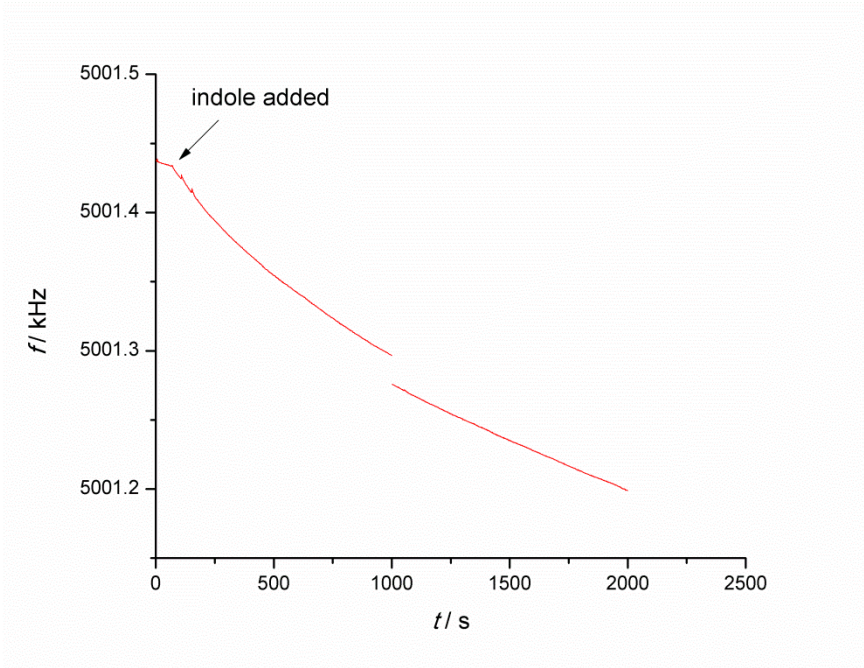

Fig. 31. Frequency response of 6-aminoindole adsorption on MWCNT-Au electrode in Ar purged 0.5 mol dm^{-3} H_2SO_4 containing 15 mmol dm^{-3} 6-aminoindole monomer at 0 V

In Fig. 31, we have the frequency response of a MWCNT film to the adsorption of 6-aminoindole from acidic solution. The potential of the electrode was held at a constant value (0 V) below the polymerization potential of the 6-aminoindole monomer to prevent disturbing effects of polymerization on the adsorption measurement. As compared to the adsorption of aniline seen in section 5.2.1, we see a much more rapid and intense adsorption

phenomena of the 6-aminoindole on MWCNT. However, it is not possible to say whether this is a selective adsorption to the surface to the MWCNTs or non-selective adsorption to both the MWCNTs and the gold surface as well due to the formation of poly(6-aminoindole) on the surface of the gold as well as can be seen in Fig. 35.

5.3.2. Polymerization of 6-aminoindole

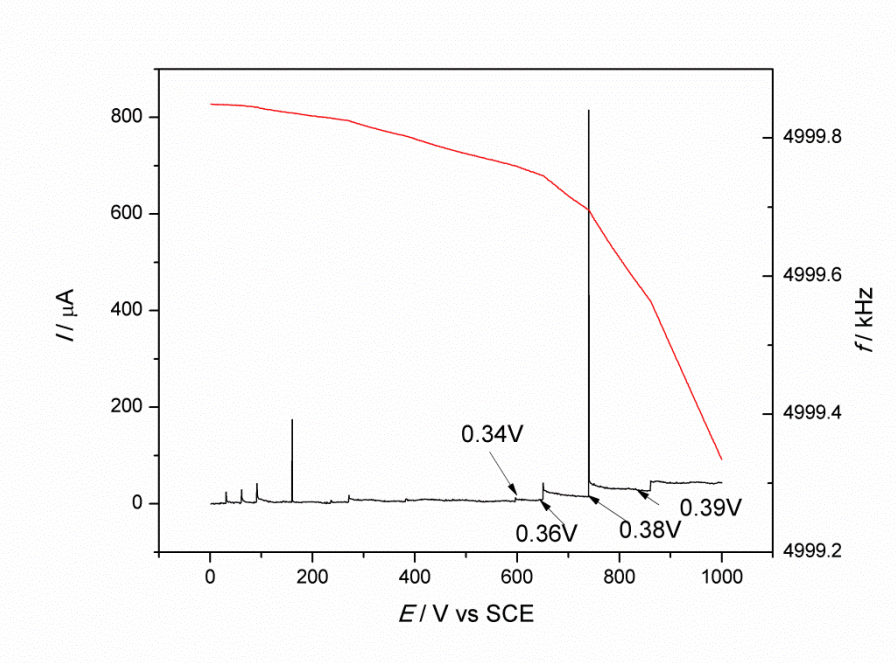

Fig. 32. Simultaneously obtained current and frequency responses to potentiostatic 6-aminoindole film generation on an Au-MWCNT electrode in contact with 0.5 mol dm^{-3} H_2SO_4. The potential was gradually stepped up with values of 0.34 V, 0.36 V, 0.38 V and finally 0.39 V

We performed chronoamperometric experiments to deposit 6-aminoindole on the surface of an Au-MWCNT electrode. The results of these experiments can be seen in Fig. 32; where the simultaneous current and frequency responses were measured at various polymerization potentials between 0.34 V and 0.39 V. It can be seen from the figure that the potential was increased stepwise until polymerization of the 6-aminoindole monomers began. The rate of deposition increased along with the potential as seen by the increasing slope of the frequency response. This rate was monitored and the polymerization was stopped before the film became too thick for a total of *ca.* 600 Hz deposition on the electrode.

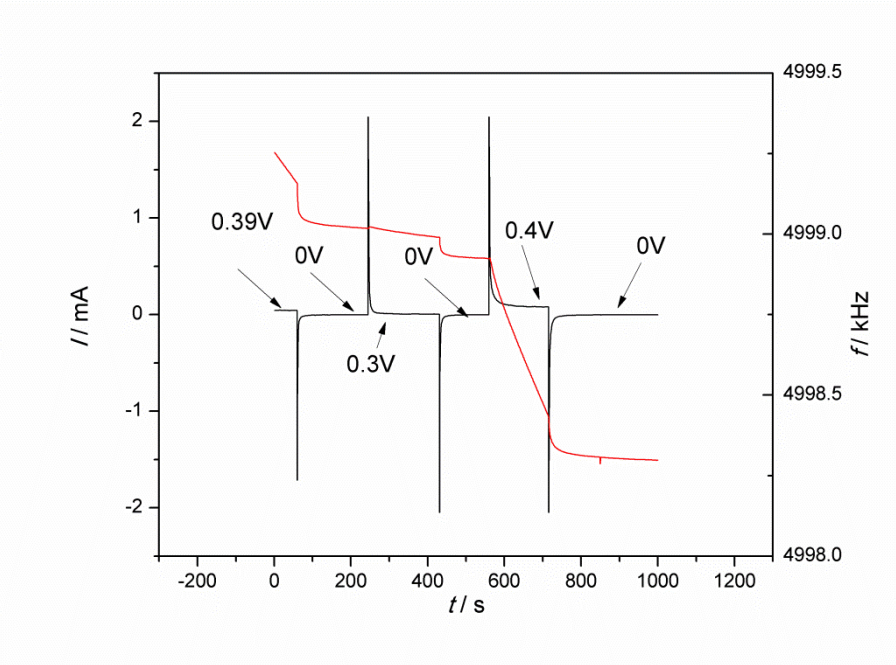

Fig. 33. Simultaneously obtained current and frequency responses to potential steps of a MWCNT-Au electrode in contact with Ar purged 0.5 mol dm^{-3} H_2SO_4 containing 15 mmol dm^{-3} 6-aminoindole monomer. A potential program of 0.39 V to 0 V to 0.3 V to 0 V to 0.4 V and back to 0 V was applied

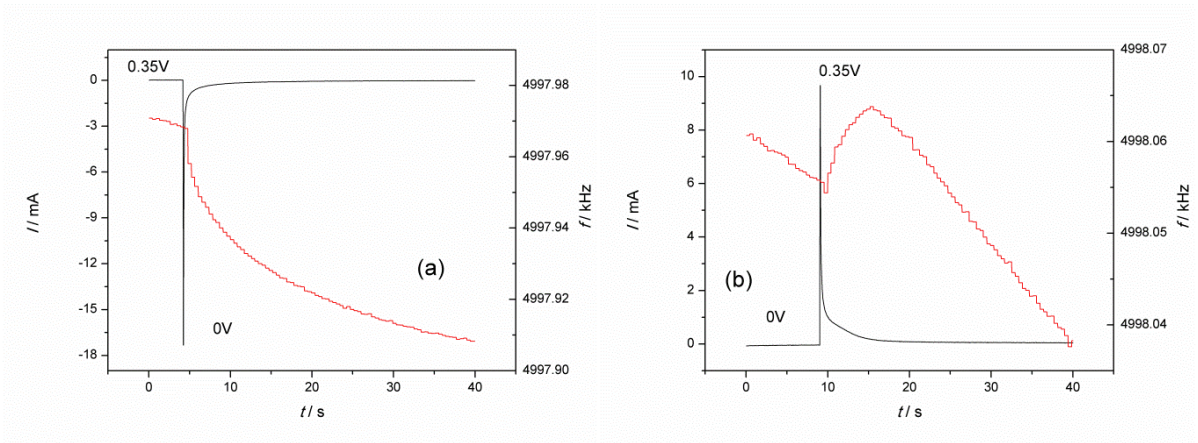

Fig. 34. Simultaneously obtained current and frequency responses of an Au-MWCNT electrode in Ar purged 0.5 mol dm^{-3} H_2SO_4 containing 15 mmol dm^{-3} 6-aminoindole monomer. Potential steps from 0.35 V to 0 V (a) and 0 V to 0.35 V (b) were performed

We performed potential steps to measure Cottrell curves for the poly(6-aminoindole)-MWCNT-Au film generated in Fig. 32 and the results of these potential steps can be seen in Fig. 33. The adsorption of 6-aminoindole is still seen by the negative slope of the frequency curve even when below the polymerization potential. Upon increasing the potential to begin

the polymerization, we obtain a time dependent current response of the unstirred 6-aminoindole solution. As the 6-aminoindole concentration at the surface of the electrode is depleted, we see a decrease in the current. In Fig. 34, we show an enlargement of the results obtained in Fig. 33. The response here is again completely diffusion controlled due to the lack of stirring of the solution. During the 0 V to 0.35 V step, the current response diminishes as the concentration of 6-aminoindole at the electrode surface is reduced and poly(6-aminoindole) is formed. The frequency response shows a slight increase just after the application of potential suggesting that there is electrolyte leaving the film due to charging of the electrode surface and repulsion of charged species. It is also possible that there are some viscosity effects caused by the formation of polymer on the surface and changes in the electric double layer that result in the observed frequency effect.

Fig. 35. A photograph of an Au-MWCNT-poly(6-aminoindole) film after generation and cycling

The gold surface in Fig. 35 exhibits a slightly reddish color not typical of a clean gold electrode surface indicating that the formation of poly(6-aminoindole) takes place not only on the MWCNTs but also on the gold surface itself. This can be contrasted to clean MWCNT in Fig. 5 and even to our PANI-MWCNT-Au film in Fig. 26 where the gold surface is a bright yellow color. In the case of the PANI electrode, it was determined via FIB-SEM measurement that the surface of the electrode was clean and free of polymerized aniline while the surface of the nanotubes were coated with a layer of PANI. The lower overpotential needed for 6-aminoindole oligomerization is the most likely cause of the effect. As was discussed previously, the overpotential of aniline oligomer formation on the gold surface is

higher than for the carbon nanotube surface. In the case of 6-aminoindole, this overpotential difference is smaller or non-existent resulting in the deposition on both the gold surface as well as the MWCNT film equally.

5.3.3. CV response of poly(6-aminoindole) MWCNT films

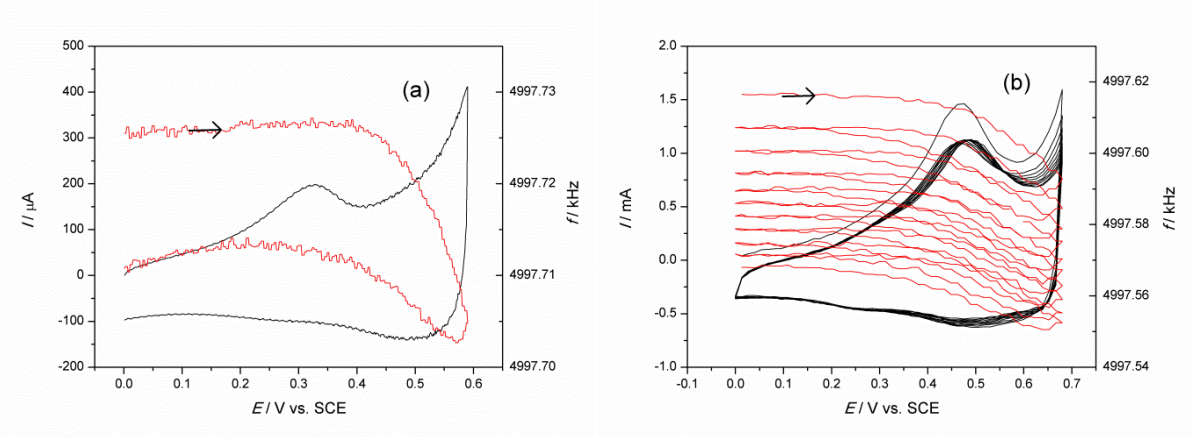

Fig. 36. The simultaneously obtained current and frequency responses of a poly(6-aminoindole)-MWCNT-Au film. The electrode was cycled using either (a) a single cycle from 0.0 V to 0.6 V at 10 mV s^{-1} or (b) 25 cycles from 0.0 V to 0.6 V at 50 mV s^{-1} both measurements were performed in Ar purged 0.5 mol dm^{-3} H_2SO_4

We simultaneously measured the frequency and current response of our poly(6-aminoindole)-MWCNT-Au film and observed the mass change seen in Fig. 36. There is an electrochemically non-reversible current response in the film with two oxidative waves. After the first wave at *ca.* 0.3 V, the deposition of 6-aminoindole begins on the surface of the electrode. The current response is seen in the large increase of the current response starting at *ca.* 0.5 V. There is a consistent frequency decrease similar to what is observed in the MWCNT films without any poly(6-aminoindole present). The effect is again most likely due to swelling of the film with water. This film swelling had a total frequency change of 340 Hz was obtained corresponding to a mass change of 6 μg over 25 cycles.

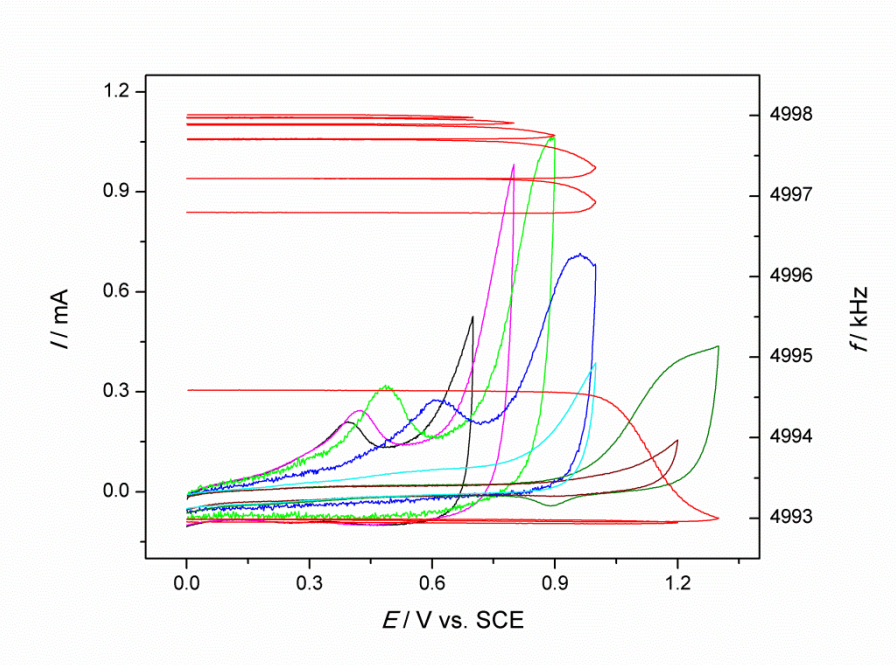

Fig. 37. Cyclic voltammograms and the simultaneously detected EQCN responses during the electrooxidation of 6-aminoindole film on Au in contact with Ar purged 0.5 mol dm^{-3} H_2SO_4. Positive potential limits were as follows: 0.55 V (2), 0.65 V (3), and 1.4 V (4-6) (three subsequent cycles) at a scan rate of 10 mV s^{-1}

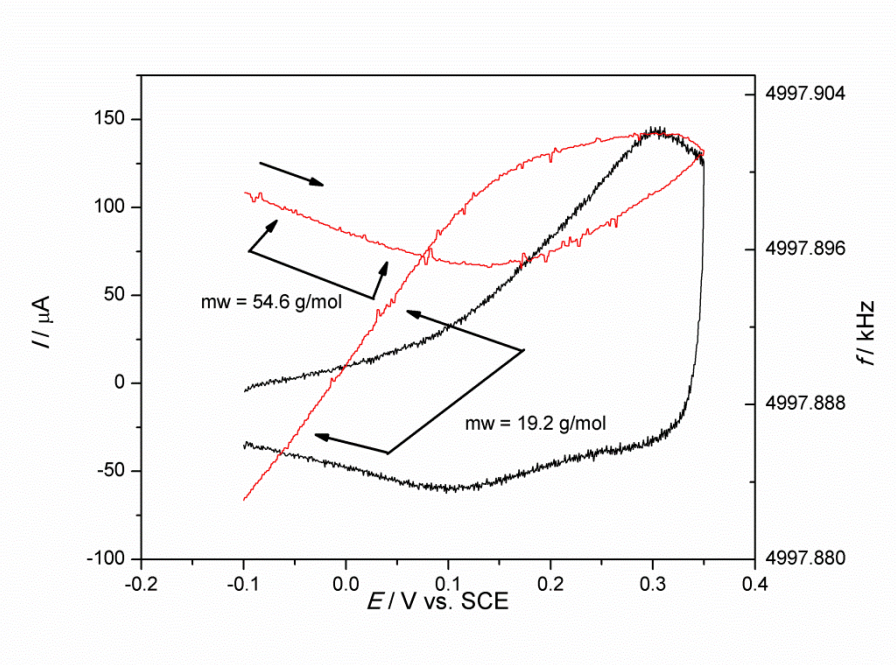

Fig. 38. Molecular mass determination for a simultaneously obtained current and frequency response of a poly(6-aminoindole)-MWCNT-Au electrode in an Ar purged 0.5 mol dm^{-3} H_2SO_4 solution at 5 mV s^{-1} from −0.1 V to 0.35 V

We performed the overoxidation of a poly(6-aminoindole)-MWCNT-Au electrode and recorded the simultaneous current and frequency responses and these data can be seen in Fig. 37. We observed the shift of the oxidative peak to higher and higher potentials upon oxidation of the film. The conductive properties of the film were destroyed by high potential cycling (above *ca.* 0.8 V) as can be seen in the final scan from 0.0 V to 1.2 V. This scan closely resembles what would be expected from a clean MWCNT-Au film suggesting that the poly(6-aminoindole) has been deactivated and causing the absence of redox waves. These findings are in accordance to previous results [56] on the overoxidation of a poly(6-aminoindole) film. We also measured the mass change of a poly(6-aminoindole)-MWCNT-Au electrode and calculated the molecular weight of the involved species from these plots. These data can be seen in Fig 38. We see that on the forward sweep, there is a mass increase corresponding to a species with molecular weight 54.6 g mol^{-1}. On the reverse sweep, we see a mass decrease corresponding to a species with a molecular weight of 19.2 g mol^{-1}. The overall process is an increase in the film mass due to swelling with water molecules.

6. Conclusions

It has been shown that MWCNT immobilized on the gold electrode of an EQCN can be activated by potential cycling applying a switching potential higher than 0.6 V. The extensive potential cycling results in an increasing capacitance and a rather high mass increase which is comparable with the original mass of the MWCNT layer. This mass increase can be assigned to the sorption of water molecules. It is mostly due to the formation of functional groups – similar to the chemical activation by oxidation in acid media – which makes the layer hydrophilic. The increased capacitance is due to the increase of the real surface area. It manifests itself also in the increase of the non-specific adsorption of the respective ions around the pzc at lower potentials.

Aniline is adsorbed on MWCNTs, and the adsorbed aniline can be oxidized to oligomeric species and polyaniline. The adsorption of aniline substantially decreases the solvent swelling effect. When the usual electropolymerization of aniline is executed by applying dissolved aniline in acid solution, polyaniline grows on the MWCNTs covered by aniline oligomers and polyaniline. By using a lower positive potential limit, i.e., a somewhat lower one than that necessary to initiate the electropolymerization on gold, the deposition of PANI occurs entirely on the nanotubes and not on the uncovered parts of the gold electrode. It is due to the

autocatalytic nature of the aniline electropolymerization since the deposition of the polymer is preferable at places when a thin layer of polyaniline is already present. In a similar way, 6-aminoindole is also adsorbed on MWCNTs at potentials below the oxidation of indole. However, when the positive potential limit is increased, the polymerization of indole proceeds not only on the MWCNTs but also on the surface of the gold as well. This indicates that there is not the same catalyzing effect of the MWCNTs on indole polymerization.

A rather high increase of the capacitance can be achieved by deposition of polyaniline. It can be attributed not only to the pseudocapacitive contribution of the deposited PANI, but a synergic effect can also be observed because the conductive polymer chains connecting the nanotubes causes enhanced conductivity of the layer. In the case of both the activated nanotubes and the MWCNT-PANI composites, reversible mass changes can be observed during cycling which are related to the motion of the charge-compensating anions. The originally 3-8 F g^{-1} specific capacitance of the MWCNTs can be increased to 40-100 F g^{-1} by electrochemical activation, by depositing polyaniline on the nanotubes 300-500 F g^{-1} can easily be reached and 500-1,000 F g^{-1} are possible with the addition of polyindole even at high charging-discharging rates.

7. Summary

Electrochemical Nanogravimetric studies of Multi-walled Carbon Nanotubes and their Composites with Conducting Polymers

Colin E Moore, M.Sc. student in Chemistry

Department of Physical Chemistry, Institute of Chemistry, Eötvös Loránd University, Budapest

Place of defense: Department of Physical Chemistry

Supervisor: **Professor Dr. György Inzelt**

Department of Physical Chemistry

This thesis is the culmination of my diploma work at ELTE. I researched properties conducting polymers including polyaniline (PANI) and poly(aminoindole) and their composites with carbon nanotubes. Results were achieved using cyclic voltammetry (CV) coupled to electrochemical quartz crystal nanobalance (EQCN) as well as scanning electron microscopy (SEM). I demonstrated that multi-walled carbon nanotubes (MWCNTs) immobilized on the gold electrode of an EQCN can be activated by potential cycling applying a switching potential higher than 0.6 V. Extensive potential cycling results in an increasing capacitance and a rather high mass increase which is comparable with the original mass of the MWCNT layer. Aniline is adsorbed on MWCNTs, and the adsorbed aniline can be oxidized to oligomeric species and polyaniline. The adsorption of aniline substantially decreases the solvent swelling effect. By using a lower positive potential limit, i.e., a somewhat lower one than that necessary to initiate the electropolymerization on gold, the deposition of PANI occurs entirely on the nanotubes and not on the uncovered parts of the gold electrode. It is due to the autocatalytic nature of the aniline electropolymerization since the deposition of the polymer is preferable at places when a thin layer of polyaniline is already present. In a similar way, 6-amino-indole is also adsorbed on MWCNTs at potentials below the oxidation of indole. However, when the positive potential limit is increased, the polymerization of indole proceeds not only on the MWCNTs but also on the surface of the gold as well. A rather high increase of the capacitance can be achieved by deposition of polyaniline. It can be attributed not only to the pseudocapacitive contribution of the deposited PANI, but a synergic effect can also be observed because the conductive polymer chains connecting the nanotubes cause enhanced conductivity of the layer.

8. References

1. Kavan L, Dunsch L (2008) Electrochemistry of carbon nanotubes. In: Topics in Applied Physics, Berlin Springer-Verl 111:567-603
2. Kavan L, Dunsch L (2011) Spectroelectrochemistry of carbon nanotubes. Chem Phys Chem 12:47-55
3. Rivas GA, Rubianes MD, Pedano ML, Ferreyra NF, Luque G, Miscoria SA (2009) Carbon nanotubes: a new alternative for electrochemical sensors. In: Nanoscience and technology series. Nova Sci Publ, New York
4. Sun G, Zhou JY, Yu F, Zhang Y, Pang JHL, Zheng L (2012) Electrochemical capacitive properties of CNT fibers spun from vertically aligned CNT arrays. J Solid State Electrochem 16:1775-1780
5. Barisci JN, Wallace GG, Baughman RH (2000) Electrochemical quartz crystal microbalance studies of single-wall carbon nanotubes in aqueous and non-aqueous solutions. Electrochim Acta 46:509-517
6. Haubner K, Luspai K, Rapta P, Dunsch L (2011) The charging of the carbon nanotube/oligothiophene interphase as studied by in situ electron spin resonance/UV-Vis-NIR spectroelectrochemistry. Phys Chem Chem Phys 13:13403-13409
7. Kalbac M, Kavan L, Dunsch L (2009) An in situ Raman spectroelectrochemical study of the controlled doping of semiconducting single walled carbon nanotubes in a conducting polymer matrix. Synth Metals 159:2245-2248
8. Feng W, Bai XD, Lian YQ, Liang J, Wang XG, Yoshino K (2003) Well-aligned polyaniline / carbon-nanotube composite films grown by in-situ aniline polymerization. Carbon 41:1551–1557
9. Huang JE, Li XH, Xu JC, Li HL (2003) Well-dispersed single-walled carbon nanotube/polyaniline composite films. Carbon 41:2731-2736
10. Wu TM, Lin YW, Liao CS (2005) Preparation and characterization of polyaniline/multi-walled carbon nanotube composites. Carbon 43:734–740
11. Cheng Q, Tang, J, Shinya N, Qin LC (2013) Polyaniline modified graphene and carbon nanotube composite electrode for asymmetric supercapacitors of high energy density. J Power Sources 241: 423-428
12. Kulkarni MV, Kale BB (2013) Studies of conducting polyaniline (PANI) wrapped-multi-walled carbon nanotubes (MWCNTs) nanocomposite and its application for optical pH sensing. Sensors Actuators B-Chem 187:407-412

13. Paul S, Choi KS, Lee DJ, Sudhagar P, Kang YS (2012) Factors affecting the performance of supercapacitors assembled with polypyrrole/multi-walled carbon nanotube composite electrodes. Electrochim Acta 78:649-655
14. Sun X, Xu Y, Wang J (2012) Electropolymerized composite film of polypyrrole and functionalized multi-walled carbon nanotubes: effect of functionalization time on capacitive performance. J Solid State Electrochem 16:1781–1789
15. Zhang L, Shi Z, Lang QH (2011) Fabrication of poly(orthanilic acid)-multiwalled carbon nanotubes composite film-modified glassy carbon electrode and its use for the simultaneous determination of uric acid and dopamine in the presence of ascorbic acid. J Solid State Electrochem 15:801-809
16. An HF, Wang Y, Wang XY, Li N, Zheng L (2010) The preparation of PANI/CA composite electrode material for supercapacitors and its electrochemical performance. J Solid State Electrochem 14:651-657
17. Bavio MA, Acosta GG, Kessler T (2014) Synthesis and characterization of polyaniline and polyaniline – carbon nanotubes nanostructures for electrochemical supercapacitors. J Power Sources 245:475-481
18. Zhang J, Kong LB, Wang B, Luo YC, Kang L (2009) In-situ electrochemical polymerization of multi-walled carbon nanotube/polyaniline composite films for electrochemical supercapacitors. Synth Metals 159: 260-266
19. Gajendran P, Saraswathi R (2008) Polyaniline-carbon nanotube composites. Pure Appl Chem 80:2377-2395
20. Peng C, Zhang S, Jewell D, Chen GZ (2008) Carbon nanotube and conducting polymer composites for supercapapcitors. Prog Natural Sci 18: 777-788
21. Mikhaylova AA, Tusseeva EK, Mayorova NA, Rychagov AY, Volfkovich YM, Krestinin AV, Khazova OA (2011) Single-walled carbon nanotubes and their composites with polyaniline. Electrochim Acta 56:3656-3665
22. Dong B, He BL, Xu CL, Li HL (2007) Preparation and electrochemical characterization of polyaniline/multi-walled carbon nanotubes composites for supercapacitors. Materials Sci Eng B 143:7-13
23. Guo DJ, Li HL (2005) Well-dispersed multi-walled carbon nanotube/polyaniline composite films. J Solid State Electrochem 9:445-449
24. Aygun A, Buthker JW, Stephenson LD, Kumar A, Mahle TK, Gewirth AA (2012) Electrochemically controlled swelling properties of nanoporous templated polypyrrole and layer by layer polypyrrole. J Electroanal Chem 684:47-52

25. Snook GA, Chen GZ, Fray DJ, Hughes M, Shaffer M (2004) Studies of deposition of charge storage in polypyrrole-chloride and polypyrrole-carbon nanotube composites with electrochemical quartz crystal microbalance. J Electroanal Chem 568:135-142
26. Inzelt G (2012) Conducting polymers - A new era in electrochemistry. 2nd edn. In: Scholz F (ed) Monographs in electrochemistry. Springer, Heidelberg Berlin
27. Inzelt G (2010) Electrochemical quartz crystal nanobalance. In: Scholz F (ed) Electroanalytical Methods: Guide to Experiments and Applications, 2nd edition, Springer, Heidelberg, pp 257–270
28. Frackowiak E, Béguin F (2001) Carbon materials for supercapacitors. Carbon 39:937–950
29. Brett CMA, Brett AMO (1993) Electrochemistry: principles, methods and applications. Oxford University Press, Oxford
30. Bard AJ, Faulkner LR (2000) Electrochemical methods. 2nd edn. JohnWiley, New York
31. Parsons R (1990) Electrical double layer: recent experimental and theoretical developments. Chem Rev 90:813
32. Trasatti S (1985) In: Silva AF (ed) Trends in interfacial electrochemistry. Proc of NATO ASI, Reidel, Dordrecht, pp 25-48
33. Wang X, Li Q, Xie J, Jin Z, Wang J, Li Y, Jiang K, Fan S (2009) Fabrication of ultralong and electrically uniform single-walled carbon nanotubes on clean substrates. Nano Letters 9:3137–3141
34. Shirakawa H, Louis EJ, MacDiarmid AG, Chiang CK, Heeger A.J (1977) Synthesis of Electrically Conducting Organic Polymers. J Chem Soc Chem Comm 474:578-580
35. Inzelt G (2008) Rise and Rise of conducting polymers. J Solid State Electrochemistry 15:1711-1718
36. Letheby H (1862) On the production of a blue substance by the electrolysis of sulphate of aniline. J Chem Soc 15:161-163
37. Baeyer A (1866) Ueber die reduction aromatischer verbindungen mittelst zinkstaub. Ann 140:295-303
38. Humphrey GR, Kuethe JT (2006) Practical methodologies for the synthesis of indoles. Chem Rev 106:2875-2911
39. Bratulescu G (2008) A new and efficient one-pot synthesis of indoles. Tetrahedron Letters 49:984-986
40. Merz A, Bard AJ (1978) A stable surface modified platinum electrode prepared by coating with electroactive polymer. J Am Chem Soc 100:3222–3223

41. Tüken T, Yazici B, Erbil M (2005) Electrochemical synthesis of polyindole on nickel-coated mild steel and its corrosion performance. Surf Coat Technol 200:2301-2309
42. Bard AJ (1994) Integrated chemical systems. A chemical approach to nanotechnology. Wiley-Interscience, New York
43. Billaud D, Maarouf EB, Hanecart E (1995) Chemical oxidation and polymerization of indole. Synth Met 69:571–572
44. Cai Z, Yang G (2010) Synthesis of polyindole and its evaluation for Li-ion battery applications. Synth Met 160:1902–1905
45. Pandey PC, Prakash R (1998) Electrochemical synthesis of polyindole and its evaluation for rechargeable battery applications. J Electrochem Soc 145:999–1003
46. Biegunski AT, Michota A, Bukowska J, Jackowska K (2006) Immobilisation of tyrosinase on poly(indole-5-carboxylic acid) evidenced by electrochemical and spectroscopic methods. Bioelectrochem 69:41–48
47. Maarouf EB, Billaud D, Hannecart E (1994) Electrochemical cycling and electrochromic properties of polyindole. Mater Res Bull 29:637–643
48. Talbi H, Maarouf EB, Humbert B, Alnot M, Ehrhardt JJ, Ghanbaja J, Billaud D (1996) Spectroscopic studies of electrochemically doped polyindole. J Phys Chem Solids 57:1145–1151
49. Talbi H, Billaud D, Louarn G, Pron A (2000) UV–vis and Raman spectroelectrochemical investigation of the redox behavior of poly(5-cyanoindole) in acidic aqueous solutions. Spectrochim Acta 56:717–728
50. Jackowska K, Kudelski A, Bukowska J (1994) Spectroelectrochemical and EPR determination of the number of electrons transferred in the redox processes in electroactive polymers. Polyindole films. Electrochim Acta 39:1365–1368
51. Nie G, Zhou L, Guo Q, Zhang S (2010) A new electrochromic material from an indole derivative and its application in high quality electrochromic devices. Electrochem Commun 12:160–163
52. Tourillon G, Garnier F (1982) New electrochemically generated organic conducting polymers. J Electroanal Chem 135:173–178
53. Waltman RJ, Diaz AF, Bargon J (1984) Substituent effect in the electropolymerization of aromatic heterocyclic compounds. J Phys Chem 88:4343–4346
54. Bartlett PN, Dawson DH, Farrington J (1992) Electrochemically polymerised films of 5-carboxyindole. J Chem Soc Faraday Trans 88:2685–2695
55. Holze R, Hamann CH (1991) Electrosynthetic aspects of anodic reactions of anilines and indoles. Tetrahedron 47:737–746

56. Berkes BB, Nemes Á, Moore CE, Szabó F, Inzelt G (2013) Electrochemical nanogravimetric study of the electropolymerization of 6-aminoindole and the redox transformations of the polymer formed in aqueous media. J Solid State Electrochem 17:3067–3074
57. Hickling A (1942) Studies in electrode polarisation. Part IV.-The automatic control of the potential of a working electrode. Trans of the Faraday Soc 38: 27–33
58. Randles JEB (1948) A cathode ray polarograph. Part II.—The current-voltage curves. Trans Faraday Soc 44:327-338
59. Sevcik A (1948) Oscillographic polarography with periodical triangular voltage. Coll Czech Chem Commun 13:349-377
60. Sauerbrey G (1959) Verwendung von schwingquarzen zur wägung dünner schichten und zur mikrowägung. Zeitschrift für Physik 155:206-222
61. McMullan D (2006) Scanning electron microscopy 1928–1965. Scanning 17:175
62. McMullan D (1988) Von Ardenne and the scanning electron microscope. Proc Roy Microsc Soc 23:283–288
64. Jusys Z, Bruckenstein S, Hillman AR (2011) New insights into the Belousov-Zhabotinski reaction derived from EQCM measurements at a gold electrode. Phys Chem Chem Phys 13:5373-5382
65. Chopra AK, Sharma AK, Kumar V (2011) Overview of Electrolytic treatment: An alternative technology for purification of wastewater. Archives of Applied Science Research 3:191-206
66. Hong KH, Chang D, Bae HS, Sunwoo1 Y, Kim JH, Kim DG (2013) Electrolytic removal of phosphorus in wastewater with noble electrode under the conditions of low current and constant voltage. Int J Electrochem Sci 8:8557-8571
67. Kim G, Igunnu ET, Chen GZ (2014) A sunlight assisted dual purpose photoelectrochemical cell for low voltage removal of heavy metals and organic pollutants in wastewater. Chem Eng J 244:411-421
68. Tsionsky V, Daikhin L, Urbakh M, Gileadi E (2004) Looking at the metal/solution interface with electrochemical quartz crystal microbalance: theory and experiment. In: Bard AJ, Rubinstein I (eds), Electroanalytical Chemistry, Marcel Dekker, New York 1-99
69. Levi MD, Sigalov S, Salitra G, Elazari R, Aurbach D (2011) Assessing the solvation number of electrolytic ions confined in carbon nanopores under dynamic charging conditions. J Phys Chem Lett 2:120-124
70. Pruneanu S, Csahók E, Kertész V, Inzelt G (1998) Electrochemical quartz crystal microbalance study of the influence of solution composition on the behaviour of poly(aniline) electrodes. Electrochim Acta 43:2305-2323

71. MacDiarmid AG (2001) "Synthetic Metals": A novel role for organic polymers (Nobel Lecture). Ange Chem Intl Edn 40:2581-2590
72. Chiang JC, MacDiarmid AG (1986) Polyaniline: protonic acid doping of the emeraldine form to the metallic regime. Synth Metals 13:193-205
73. Feast WJ, Tsibouklis J, Pouwer KL, Groenendaal L, Meijer EW (1996) Synthesis, processing and material properties of conjugated polymers. Polymer 37:5017-5047

9. DECLARATION

Name: **Colin E. Moore**

ELTE Természettudományi Kar (Faculty of Science): Vegyész M.Sc. (chemistry major M.Sc.)

Neptun code: DBNZNF

Title of the diploma work: **Electrochemical Nanogravimetric studies of Multi-walled Carbon Nanotubes and their Composites with Conducting Polymers**

Hereby I declare that my diploma work is based on my own research. I applied the requirements posed for correct citation of the work of others. There is not any part of the dissertation in that others' works (papers, books, lectures) are used without the due referencing.

Budapest, May 13, 2014

Signature:_____